Reversible ammonia-based and liquid organic hydrogen carriers for high-density hydrogen storage: Recent progress

Makepeace, Joshua W.; He, Teng; Weidenthaler, Claudia; Jensen, Torben R.; Chang, Fei; Vegge, Tejs; Ngene, Peter; Kojima, Yoshitsugu; de Jongh, Petra E.; Chen, Ping

Total number of authors:
11

Published in:
International Journal of Hydrogen Energy

Link to article, DOI:
10.1016/j.ijhydene.2019.01.144

Publication date:
2019

Document Version
Publisher's PDF, also known as Version of record

INTERNATIONAL JOURNAL OF HYDROGEN ENERGY 44 (2019) 7746–7767

Available online at www.sciencedirect.com

ScienceDirect

journal homepage: www.elsevier.com/locate/he

Reversible ammonia-based and liquid organic hydrogen carriers for high-density hydrogen storage: Recent progress

Joshua W. Makepeace [a,*], *Teng He* [b], *Claudia Weidenthaler* [c], *Torben R. Jensen* [d], *Fei Chang* [e], *Tejs Vegge* [f], *Peter Ngene* [e], *Yoshitsugu Kojima* [g], *Petra E. de Jongh* [e], *Ping Chen* [b], *William I.F. David* [a,h]

[a] *Inorganic Chemistry Laboratory, University of Oxford, South Parks Road, Oxford, OX1 3QR, United Kingdom*
[b] *Dalian Institute of Chemical Physics, Chinese Academy of Sciences, Dalian, 116023, People's Republic of China*
[c] *Department of Heterogeneous Catalysis, Max-Planck-Institut für Kohlenforschung, Kaiser-Wilhelm-Platz 1, Mülheim an der Ruhr, D-45470, Germany*
[d] *Interdisciplinary Nanoscience Center (iNANO) and Department of Chemistry, Aarhus University, Langelandsgade 140, 8000 Aarhus C, Denmark*
[e] *Inorganic Chemistry and Catalysis, Debye Institute for Nanomaterials Science, Utrecht University, Universiteitsweg 99, 3584CG, the Netherlands*
[f] *Department of Energy Conversion and Storage, Technical University of Denmark, Fysikvej, DK-2800, Kgs. Lyngby, Denmark*
[g] *Natural Science Centre for Basic Research and Development, Hiroshima University, 1-3-1 Kagamiyama, Higashi-Hiroshima, 739-8530, Japan*
[h] *ISIS Neutron and Muon Source, Rutherford Appleton Laboratory, Harwell Campus, Didcot, OX11 0QX, United Kingdom*

ARTICLE INFO

Article history:
Received 21 September 2018
Received in revised form
9 January 2019
Accepted 14 January 2019
Available online 13 February 2019

ABSTRACT

Liquid hydrogen carriers are considered to be attractive hydrogen storage options because of their ease of integration into existing chemical transportation infrastructures when compared with liquid or compressed hydrogen. The development of such carriers forms part of the work of the International Energy Agency Task 32: Hydrogen-Based Energy Storage. Here, we report the state-of-the-art for ammonia-based and liquid organic hydrogen carriers, with a particular focus on the challenge of ensuring easily regenerable, high-density hydrogen storage.

Introduction

Hydrogen and hydrogen-based fuels remain a key part of the portfolio of energy storage methods which are needed to ensure a transition to a renewable electricity-based energy sector. The hydrogen energy cycle is based on the interconversion of water and hydrogen as a way of storing and releasing energy from renewable electricity. The technical

* *Corresponding author.*
E-mail addresses: josh.makepeace@chem.ox.ac.uk (J.W. Makepeace), bill.david@stfc.ac.uk (W.I.F. David).
https://doi.org/10.1016/j.ijhydene.2019.01.144

challenges associated with the implementation of a large-scale hydrogen energy system have been divided into four main areas: hydrogen production, distribution, storage and utilisation [1]. In hydrogen storage, a wide range of hydrogen carriers, particularly solid materials, have been explored as alternatives to the compression or liquefaction of pure hydrogen in the context of hydrogen fuel cell vehicles [2–8]. However, most of the explored materials only achieve reversible, high-density hydrogen storage under reaction conditions far from the operating parameters of a vehicle-based system [9,10]. As a result, hydrogen storage in current and prototype hydrogen fuel cell vehicles is almost exclusively based on compression: 70 MPa hydrogen gas in the GM HydroGen3 [11], Toyota Mirai [12], Honda Clarity [13], Hyundai ix35 [14], Audi h-tron quattro [15], and Mercedes-Benz GLC-F-CELL [16], and 35 MPa hydrogen gas in the Riversimple Rasa [17].

Although the development of hydrogen storage technology that meets the demanding requirements of on-board hydrogen delivery [18] remains a key goal, it is not the only use to which hydrogen storage can be applied. This diversity of applications was recognised in the framing of International Energy Agency Task 32 to include stationary energy storage applications. In this article, we will articulate the potential for liquid hydrogen carriers to be used as stationary energy stores and in the distribution of hydrogen alongside their development for vehicular use. In these other scenarios, the 70 MPa compressed hydrogen storage option is prohibitively expensive [19,20], and therefore alternative hydrogen storage approaches will be needed.

Some key characteristics of a selection of liquid hydrogen carriers are shown in Table 1, alongside those of 70 MPa compressed hydrogen gas and liquid hydrogen, for comparison. A survey of these properties quickly reveals some of the key advantages of liquid carriers over the compression/liquefaction of pure hydrogen. The volumetric hydrogen densities (considering the material only) of these carriers reach as high as 150% of the value for liquid hydrogen in the case of liquid ammonia. Critically, these high hydrogen densities are achieved under ambient or near-ambient storage conditions. This is in contrast to the high pressures or low temperatures required to achieve practically useful volumetric hydrogen density with pure hydrogen. From a safety perspective, the liquid carriers listed in Table 1 all have narrower explosive limits in air than pure hydrogen, though have toxicity issues which must be addressed to ensure safe use.

A working energy network system requires energy storage technologies at many different scales of energy, power and storage duration. High volumetric energy density, under modest storage conditions, makes liquid hydrogen carriers attractive options for large-scale and longer-duration energy storage. In these cases, the lower round-trip efficiency of hydrogen production and storage relative to other energy-storage technologies is compensated by its high energy density, transportability and low self-discharge rate [23,24]. This type of energy storage may be required for the inter-seasonal balancing of energy demand in areas with large seasonal variations in energy use. For example, primary energy use in the United Kingdom between the winter and summer has varied on average by over 200 TWh over the past 20 years [25]. The synthesis and storage of hydrogen during times of excess electricity could then displace much of the large natural gas consumption during the UK winter, which accounts for most of this seasonal variation [25]. In this example, 10–20 Mt of hydrogen would need to be stored across the winter, depending on the efficiency of the energy release technology. Although geological hydrogen storage may be cheapest in locations where it is available [19,20,26], in other cases, conversion to a liquid carrier is likely to be the most effective means of storing of hydrogen at large scale [19]. Chemical energy storage is also considered to be a viable model for storing renewable energy from "stranded" renewable power generation, where grid connections are not economically viable [27–29].

The uses of hydrogen storage in stationary energy storage outlined above are in addition to the well-documented potential for hydrogen to contribute to the decarbonisation of transport, which currently constitutes around 35% of all energy end use [30]. Infrastructure for the distribution of hydrogen for transport is a key limiting step for the roll-out of fuel cell vehicles, and requires significant capital investment [31,32]. Liquid hydrogen stores have the potential to significantly alleviate cost associated with the distribution of

Table 1 – Comparison of some key properties of a range of reversible liquid hydrogen carriers with compressed and liquid hydrogen.

Storage method	Storage conditions	Hydrogen density (kgH_2/m^3)	H_2 release conditions	Explosive limits (%vol in air)	PEL[a] (ppmv)	Vapor pressure (MPa @ 298 K)
Compressed H_2	70 MPa	42	Pressure release	4–75	N/A	–
Liquid H_2	20.28 K	70	Evaporation	4–75	N/A	–
Liquid NH_3	239.81 K @ 0.1 MPa	121	Catalytic T > 400 °C	15–28	50	1.1
	1 MPa @ 298 K	107				
Methylcyclohexane (MCH)	Ambient	47	Catalytic T > 300 °C	1.2–6.7 (MCH) 1.2–7.1 (Toluene)	500 200	0.006
Methanol	Ambient	100	Catalytic T > 200 °C	6.7–36	200	0.017
Formic acid	Ambient	53	Catalytic T > 50 °C	18–34	5	0.006

[a] Permitted Exposure Limit, Occupational Safety and Health Administration, U.S. Department of Labor. Given as 8-h time weighted average concentrations [21,22].

hydrogen because of their straightforward storage and applicability to existing fuel transport methods. This allows larger quantities of hydrogen to be transported in each truck/ship load. This is particularly important when considering supply models such as those in active development for Japan (Fig. 1), where it is envisaged that hydrogen will be produced in regions with low-cost renewable electricity (e.g. Australia and the Middle East) and shipped to Japan for use as a fuel. The hydrogen storage methods under active consideration are liquid hydrogen, ammonia, methylcyclohexane and methane [33]. In this way, liquid hydrogen carriers have the potential to enable global hydrogen trade.

There are a number of different models for the involvement of liquid carriers in future hydrogen infrastructures:

- Large stocks of carrier transported by ship could be dehydrogenated at ports or in other centralised facilities and then distributed as pressurised or liquefied hydrogen.
- Dehydrogenation could be performed at hydrogen refuelling stations. It has been suggested that carriers could be tailored to deliver hydrogen at elevated pressure [34–36], reducing the reliance on compressors, which dominate the capital cost of refuelling stations [37]. Metal hydrides are also being explored for the production of compressed hydrogen [38].
- Liquid hydrogen carriers could be used for on-board delivery of hydrogen to a fuel cell, as has been the focus for solid-state hydrogen stores. This application is currently furthest from technical deployment due to the difficulties associated with on-board dehydrogenation and the safety issues associated with the carriers themselves.

In each of these applications, the requirements for hydrogen storage and release in a liquid carrier may vary. However, it is reasonable to state that achieving reversible hydrogen storage under moderate conditions is a key goal in the development of all liquid hydrogen carriers. Here, we will focus on recent research highlights in realising the potential of ammonia-based and liquid organic hydrogen carriers. The review does not consider carriers where hydrogen release is also accompanied by carbon dioxide release, of which formic acid and methanol have been most widely discussed. The reader is directed to several recent reviews in those areas [36,39–41]. Likewise, the hydrolysis of sodium borohydride and solution-based dehydrogenation of ammonia borane are not considered here. While aqueous solutions of these materials have comparable hydrogen storage density to methylcyclohexane [42], their hydrolysis results in the formation of a heterogeneous mixture of products containing strong B–O bonds which require harsh conditions to regenerate the starting materials [41,43,44]. Water must also be evaporated from the hydrolysed product before regeneration, making use of these solutions energy intensive and costly [45]. While much research has focussed on catalyst development for hydrogen release [46], relatively little work is published on the issues of regeneration [45].

Ammonia

Ammonia is among the most important synthetic chemicals; its industrial-scale production is credited with growing the food required to feed roughly half the current human population [47]. However, despite its very high volumetric hydrogen density (see Table 1) and mature synthesis and distribution infrastructure, ammonia has not featured prominently among the discussion of likely hydrogen carriers in recent decades. This partly relates to a U.S. Department of Energy decision in 2006 not to fund research into on-board hydrogen delivery from ammonia due to stated concerns over the high temperature of ammonia decomposition, the size and cost of catalytic reactors, poisoning of Polymer Electrolyte Membrane (PEM) fuel cells by residual ammonia, and safety issues [48].

Despite these concerns, the potential for ammonia to contribute significantly to a hydrogen-based energy system has been highlighted in a number of perspective articles in the literature [49–53]. In recent years, interest in its use in energy applications has become more widespread – some of this interest is likely to be as a result of the aforementioned effort by the Japanese government to establish a hydrogen trade sector based on the synthesis of reversible liquid hydrogen carriers in locations with abundant renewable power [33]. Indeed, the construction of two pilot 'green' ammonia production facilities is planned in Australia over the next few years, representing the first steps in the development of this hydrogen export model [54,55].

Ammonia is attractive as a way of storing energy from renewables in part because of its flexibility. It can be used as a hydrogen carrier, a direct fuel for combustion and fuel cells [56–58], or sold in its current use as a fertiliser feedstock. Indeed, recent modelling suggests that ammonia produced from renewables is already cost-competitive with traditional production [29,59], with the added incentive of reducing the carbon footprint of an industry which is estimated to account for around 1.5% of global greenhouse gas emissions [60]. In considering here the use of ammonia as a hydrogen carrier, the areas of concern outlined in the 2006 U. S. DOE report are a

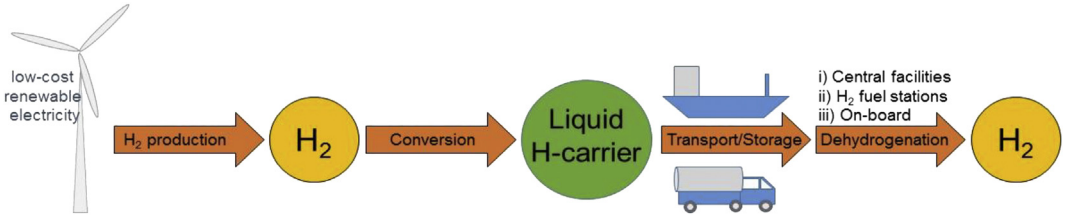

Fig. 1 – A schematic process diagram of the role of liquid hydrogen carriers in facilitating the use of hydrogen for energy storage.

useful way of structuring the discussion of recent research progress. We shall outline approaches to the development of catalysts for the synthesis and decomposition of ammonia under milder reaction conditions, efforts to address toxicity concerns through the storage of ammonia in the solid state and preventing the exposure of fuel cells to ammonia through absorbent and membrane approaches.

Ammonia synthesis

The industrial production of ammonia through the conventional Haber-Bosch process consumes 1–2% of the annual global energy demand and generates about 2.9 metric tons of CO_2 per metric ton of NH_3 produced [61]. While a majority of these emissions arise from the synthesis of hydrogen, ammonia production by the Haber-Bosch process requires high reaction temperatures (350–500 °C) and pressures (15–35 MPa of H_2 and N_2 with a ratio of 3:1) [62,63]. An improvement in the rate of this process (i.e., the development of ammonia synthesis catalysts), so that it could be operated at lower temperatures (or pressures), could have significant impact on both the economy and the environment. For example, calculations on an industrial ammonia synthesis process indicated that decreasing the equilibrium synthesis temperature from 440 °C to 360 °C would save around 1 GJ/MT of ammonia produced [64]. Enabling ammonia synthesis at milder conditions may also facilitate small-scale ammonia production linked to renewable power sources through more flexible operation. In this section, we highlight recent innovations in catalyst materials as well as advances in alternative production process to the Haber-Bosch process, specifically, electrochemical ammonia synthesis.

Thermal ammonia production

It has been reported that the activities of transition metals in catalyzing NH_3 synthesis exhibit a volcano-type dependence of the activity on the chemisorption energy of N (as shown in Fig. 2) [65]. This dependency can be explained by the Brønsted-Evans-Polanyi (BEP) and scaling relations, because a linear correlation between the N_2 dissociation energy and adsorption energy of N has been clearly demonstrated [65,66]. This linear relationship provides a theoretical guideline for the search for efficient catalysts within the volcano-type plot; efficient NH_3 synthesis requires a catalyst which strongly activates the reactants (N_2 and H_2), but also a relatively weak binding of the intermediate species and products [65,67]. Therefore major effort to achieve ammonia synthesis at low temperatures (i.e., 150–400 °C) has mainly focused on mitigating the N adsorption energy, boosting the electron donation effect, and more recently, new approaches to breaking the scaling relation. We highlight these recent advances in the following section.

Fe and Ru are the best single-metal catalysts because of their moderate adsorption energy for N_2 [65]. Combining a transition metal at the left side of the volcano-type plot with another one at the right side could be an effective way to approach the optimal N adsorption energy. In 2000, a report proposed ternary nitrides (Fe_3Mo_3N, Co_3Mo_3N and Ni_2Mo_3N) as a novel class of NH_3 synthesis catalysts [68]. Especially, Cs promoted Co_3Mo_3N gives higher activity than that of the industrial catalyst KM1 (Fe-based catalyst with promoters such as K_2O, CaO, Al_2O_3). Because Co adsorbs N_2 too weakly and Mo adsorbs N_2 too strongly, the outstanding performance of Co–Mo alloys is attributed to the moderate adsorption energy of N on Co–Mo. Recently, Hargreaves et al. examined the role of lattice nitrogen in Co_3Mo_3N using isotopic ($^{14}N/^{15}N$) experiments and computational modelling, demonstrating the lattice nitrogen (^{14}N) in the ternary nitride exchanges with ^{15}N in the gas phase, and that NH_3 synthesis using Co_3Mo_3N occurs via a Mars-van Krevelen type mechanism (as shown in Fig. 3a) [69–71]. Co_3Mo_3N was converted into Co_6Mo_6N under a hydrogen flow at ambient pressure to generate NH_3. Based on this concept, a series of ternary nitrides have been studied as nitrogen transfer agents to produce NH_3 by directly reacting with H_2. Co-doped tantalum nitride was found to be highly active, with 52% of the nitrogen in the nitride reacting with H_2 to yield NH_3 [72]. The addition of Co, Fe or K to manganese nitride only promotes the lattice nitrogen depletion to form N_2. However, adding a small amount of Li can improve the hydrogenation rate of lattice nitrogen in Mn_3N_2 at 300 °C [73].

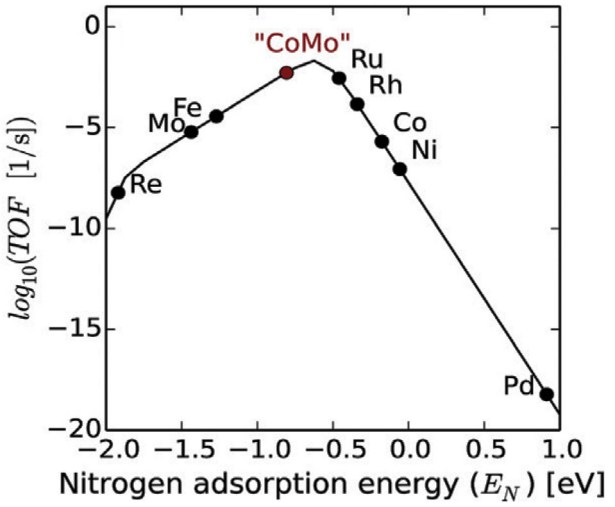

Fig. 2 – Volcano-type activity curve of ammonia synthesis. Rate shown as a function of the nitrogen adsorption energy on different transition metals, which implies there is an optimum for the nitrogen adsorption energy. Reproduced with permission from [65]. Copyright 2015 Elsevier.

Next to changing the strength of the N adsorption energy by using alloys that form nitride compounds, the addition of electronic promoters such as alkali or alkaline earth metal oxides can weaken the N≡N bond, and thus improve the activity of transition metals [74]. However, the promotion is still not sufficient to generate NH_3 under mild conditions. Hosono et al. employed an inorganic electride compound (C12A7:e^-: a crystal of $Ca_{24}Al_{28}O_{64}$ with four cavity-trapped electrons serving as anions) as a catalyst support. Because the work function of C12A7:e^- is 2.3 eV lower than that of Ru, this electride can act as an efficient electron donor for Ru [75]. The Ru/C12A7:e^- catalyst with particle size of Ru around 8.5 nm shows an activity that is two orders of magnitude larger than that of the Cs promoted Ru/MgO catalyst. Kinetic analysis and infrared spectroscopy revealed that C12A7:e^- enhances the electron back donation and N_2 dissociation. As a result, the

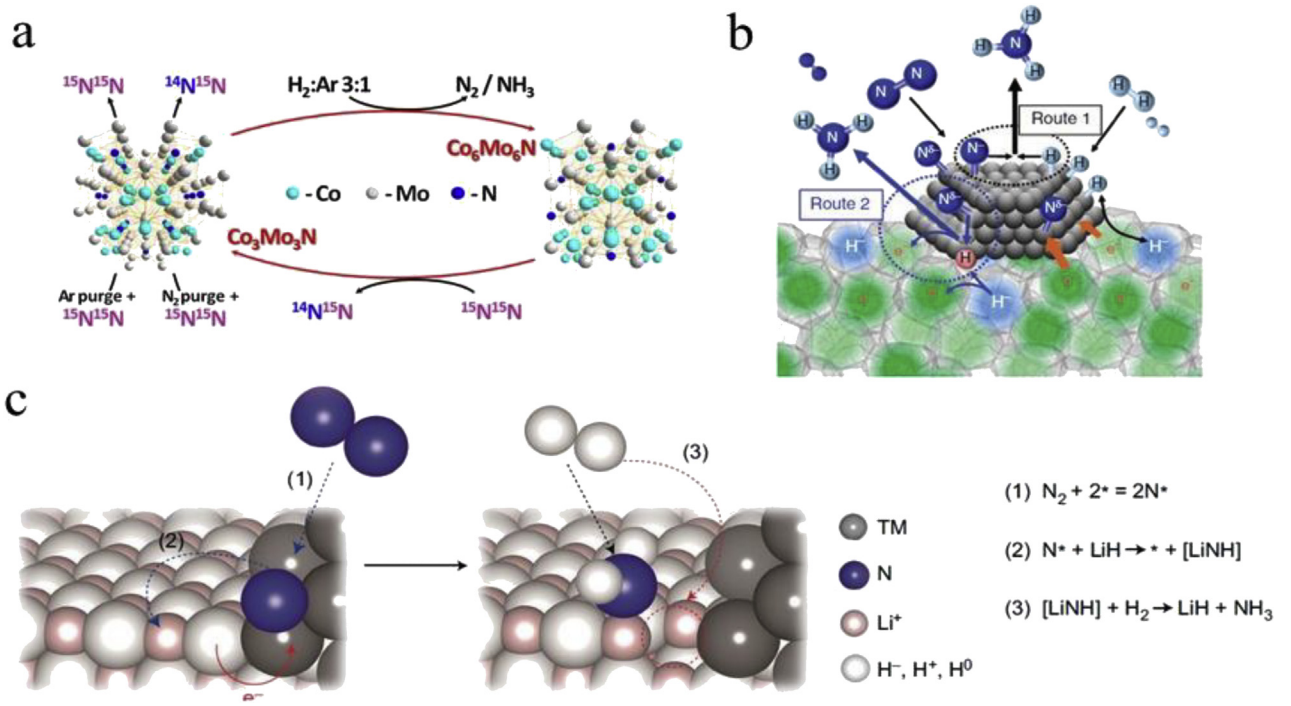

Fig. 3 – (a), Ammonia synthesis using Co_3Mo_3N catalyst occurs via a Mars-van Krevelen type mechanism. Reproduced with permission from [71]. Copyright 2013 American Chemical Society; (b), Ammonia formation mechanism over Ru/C12A7:e^- catalyst. Reproduced with permission from [76]. Copyright 2015 Nature Publishing Group; (c), Relayed ammonia synthesis mechanism for 3d-transition metal-LiH composite catalyst. Reproduced with permission from [67]. Copyright 2016 Nature Publishing Group.

hydrogenation of N atoms rather than the dissociative adsorption of N_2 over Ru is now the rate determining step [76]. Fig. 3b shows the proposed reaction mechanism over Ru/C12A7:e^-. NH_3 can be formed in two ways: via the Langmuir–Hinshelwood mechanism or by direct reaction of N adatoms with H radicals. Because the electride C12A7:e^- can reversibly store hydrogen in the form of H^-, poisoning of the Ru surface by adsorbed hydrogen atoms was suppressed. In a more recent work, a new electride Y_5Si_3 was also explored for ammonia synthesis by Hosono's group [77]. 7.8 wt% Ru loaded Y_5Si_3 catalyst exhibits an NH_3 formation rate of 1.9 mmol/g/h under the condition of 0.1 MPa and 400 °C, which is even higher than that of Ru/C12A7:e^- (0.7 $mmolg^{-1}h^{-1}$). As with C12A7:e^-, the strong electron-donating ability of Y_5Si_3 to Ru promotes N_2 dissociation and reduces activation energy of NH_3 synthesis. They showed that the performance of Ru/Y_5Si_3 did not degrade, even if the support Y_5Si_3 was submersed into water before use or if 3 vol% of water vapor pressure was introduced into the reaction gas. This is unlike other catalysts, such as nitride or hydride-based catalysts, where chemical stability against air and water is a major problem. These features may make Ru/Y_5Si_3 a promising candidate for practical application.

A relatively new class of NH_3 synthesis catalysts is aimed at breaking the scaling relationship by providing two different active sites. Chen et al. proposed LiH as a second active centre for N hydrogenation and subsequent NH_3 desorption, so that the NH_3 formation rate would no longer solely dependent on transition metals [67]. LiH can act as a strong reducing agent and remove activated nitrogen atoms from the transition metal or its nitride to form $LiNH_2$. $LiNH_2$ further splits H_2 to give off NH_3 and thereby regenerates LiH. This subsequent catalysis over two different active centers is depicted in Fig. 3c. At 300 °C, catalytic activities of 3d-transition metals (V, Cr, Mn, Fe, Co and Ni)–LiH composite catalysts are 1-4 orders of magnitude higher than those of single transition metal catalysts and some of the catalysts outperform the reference Cs–Ru/MgO catalyst. These composite catalysts have apparent activation energies that are very close to the E_a value (49 kJ mol^{-1}) of the hydrogenation of $LiNH_2$, suggesting that the hydrogenation of $LiNH_2$ is now the rate determining step. A similar high activity was reported for CNTs supported BaH_2–Co catalysts [78], and $Ca(NH_2)_2$ supported Ru catalysts [79]. The addition of barium-doped $Ca(NH_2)_2$ to Ru nanoparticles with a mean size 2.7 nm can improve the NH_3 synthesis activities significantly, which are 2 orders of magnitude higher that of Cs–Ru/MgO below 300 °C [80]. Nano sized Ru–Ba core-shell structures were formed during catalytic reaction, which possibly account for the superior performance. A recent paper discussed that alkali or alkaline earth hydrides, including LiH, BaH_2, KH, CaH_2, and NaH, can increase the catalytic activity of manganese nitride by several orders of magnitude [81]. Alkali and alkaline earth metal imides can function as nitrogen carriers that mediate ammonia production via a two-step chemical looping process: Firstly, N_2 is fixed through the reduction of N_2 by alkali or alkaline earth metal hydrides to form imides; Secondly, the imides are hydrogenated to produce NH_3 and regenerate the metal hydrides. This chemical loop process mediated by BaNH and catalyzed by Ni produces NH_3 at 100 °C and atmospheric pressure [82]. These results demonstrate that the cooperation

of transition metals and alkali or alkaline earth hydrides creates an energy-efficient pathway that allows NH_3 synthesis at lower temperatures.

As discussed above, recent studies for ammonia synthesis catalysts are dedicated to modifying the electronic structures of transition metals under the governing of scaling relations or break the scaling relation by providing two different active sites. Ternary nitrides have a comparable activity with the industrial catalysts and can even produce NH_3 at ambient pressure. Electride-supported Ru catalysts boost the N_2 activation and surpass the H_2 poisoning (an obstacle for industrial Ru-based catalysts working under high H_2 pressures). Transition metal-hydridecatalysts can separate the N_2 activation and hydrogenation or desorption steps to achieve low temperature catalysis. These encouraging results promote the search for practical low-temperature ammonia synthesis catalysts.

Electrochemical ammonia production

Electrochemical reduction of dinitrogen into ammonia at near ambient conditions represents a key enabling technology, which would accelerate the transition to an energy and chemical infrastructure based on electrical energy from renewable sources. Small-scale decentralized plants could accommodate the intermittency of, e.g., wind and solar energy, and produce ammonia for both fertiliser production and for energy storage purposes [50]. Such devices could easily be combined with safe storage solutions, where the produced ammonia can be stored safely and reversibly at high density in benign, low-cost metal halide salts [83,84], but until now, efficient and selective electrocatalysts for the nitrogen reduction reaction (NRR) have remained elusive.

It has been shown using density functional theory (DFT) calculations that certain metal nitrides, e.g. vanadium and zirconium nitride [85,86], can produce ammonia at potentials as low as −0.5 V vs. RHE, but the stability of the nitrides under reaction conditions and low Faradaic Efficiencies (FE) due competing hydrogen evolution reaction (HER) remain a challenge [87]. DFT calculations have also shown that nanostructuring the nitride catalysts can lead to improve performance [88–90], which has recently been confirmed experimentally for VN [91] and Mo_2N [92] nanowires.

A large number of different materials and approaches for electrochemical nitrogen reduction have been proposed, see e.g. Ref. [93] and references therein, but common for all are the low FE and ppb/ppm yields of ammonia, which makes quantitative ammonia detection a substantial challenge and the need for ^{15}N labelled control experiments to confirm the origin of the nitrogen essential.

Two lithium-mediated approaches have recently been proposed; a lithium-ion conductor approach by Han et al. [94] and a lithium-nitride cycling scheme by Nørskov et al. [95], where the latter holds promise of economic viability; in particular, if suitable and less thermodynamically stable nitride species are identified. The use of aprotic electrolytes was also recently proposed by MacFarlane et al. to limit the availability of protons and suppress HER [96,97] and inspiration from secondary Zn-air batteries for suppression of HER by synergistic doping [98], may also hold promise.

To overcome the massive challenges involved, it is evident that a close coupling between theory and experiment is needed in order to identify more efficient NRR electrocatalysts [63].

Ammonia decomposition

The release of hydrogen from ammonia under modest reaction conditions is one of the key challenges of the implementation of ammonia-based hydrogen storage. This challenge requires a broadening of the traditional focus of ammonia catalyst development – the synthesis of ammonia at large scale in high-pressure reactors – towards the goal of hydrogen production at high rates and moderate (<500 °C) temperatures [99,100]. The precise application of ammonia decomposition (e.g. forecourt decomposition, on-board vehicular H_2 production) and the extent of ammonia decomposition required for the power generation technology (Fig. 4) will determine the precise activity characteristics required for the catalysts. This emphasises the requirement for the development of a wide range of catalyst materials.

Transition metal catalysts

The decomposition of ammonia over transition metal based catalysts has a history which goes back to the early times of ammonia synthesis. Several reviews have been published which cover all important aspects of catalyzed ammonia decomposition and highlight potential new research fields [100–103].

The discovery of the NH_3 synthesis (Haber-Bosch process) by Fritz Haber around one hundred years ago had a tremendous influence on the development of the chemical industry [104]. However, not only the synthesis but also the decomposition of NH_3 over iron and ruthenium based catalyst, which in fact are used for the ammonia synthesis, has been studied [105–108]. Most publications in the first decades focus more on kinetic aspects of iron and ruthenium

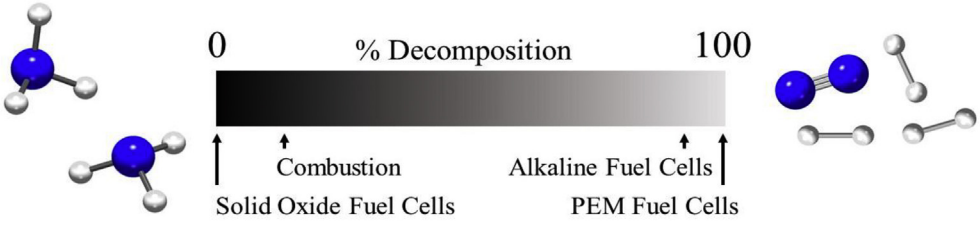

Fig. 4 – Indicative ammonia decomposition levels required for different power generation technologies.

catalysts than on a systematic scan of additional potential decomposition catalysts [109–114]. Later, the search for efficient decomposition catalysts was extended to other transition metals such as Ni, W, Mo, or Co, and also to supported precious metals [115,116].

Based on the excellent properties of Ru as an ammonia synthesis catalyst, the performance of transition metals in general for the decomposition reaction was evaluated. Several aspects were identified to be crucial for the activity of the decomposition catalysts: type of (a) active metal and (b) support, (c) surface area and particle size, (d) catalyst dispersion, and (e) the role of promotors. Choudhary et al. investigated supported metal catalysts in ammonia decomposition and observed a decrease of the ammonia conversion in the following order Ru > Ir > Ni [117]. A comparison of the behavior of Ru, Rh, Pt, Pd, Ni, and Fe as active components identified Ru among other metals as most active catalyst [118]. Catalytic testing of Ru prepared on different supports (carbon nanotubes (CNT), activated carbon (AC), Al_2O_3, MgO, ZrO_2, and TiO_2) revealed that Ru on CNTs exhibits the highest conversion of ammonia.

Whether a support has a positive effect on the ammonia decomposition is strongly dependent on the nature and structure of the support materials. CNTs and activated carbon (AC) facilitate a high dispersion of Ru on the surface and prevent particle growth of the active catalyst [118,119]. High dispersion has a positive influence on the stability of the catalyst and therewith on the catalytic activity. Nevertheless, even though high catalyst dispersion is beneficial, several studies showed that for very small Ru particles the turn-over-frequency (TOF) is significantly lower than for larger Ru particles [120,121]. Over-dispersed catalysts may result in too small catalyst particles, which do not provide enough space for the recombination of N atoms to N_2 molecules [122]. Furthermore, Li et al. investigated the importance of the structure of different carbon supports such as CNTs, AC, mesoporous carbon (CMK-3), graphitic carbon (GC), and carbon black (CB). The catalytic activity decreases from Ru/GC > Ru/CNTs > Ru/CB > Ru/CMK-3 > Ru/AC [122]. Within this order the degree of graphitization is decreasing. Conductive supports facilitate the electron transfer from promoter or support to the active metal catalysts which explains changes in catalytic activity. Yin et al. also related improved activities of Ru catalysts to an increased basicity of the support material [118]. The recombinative desorption of nitrogen from the surface appears to be the rate-limiting step in ammonia decomposition [122] but stronger basicity seems to support N_2 desorption [118]. The combination of basicity with good electronic conductivity of the support appears to be essential for the development of efficient catalysts for ammonia decomposition.

Alkali, alkaline earth, or rare-earth ions added as promoters can further enhance the decomposition of ammonia. Among all studied promoters K, Cs, and Ba are the most beneficial and therefore also the most studies ones [123–127]. Promoters may prohibit sintering of the active metal catalysts as known for ammonia synthesis and the modification of CNTs with KOH was reported to decrease of the N_2 desorption temperatures [118]. Decomposition of ammonia on metals occurs in a stepwise sequence starting with the adsorption of ammonia on the metal followed by stepwise dehydrogenation of NH_3 and recombinative desorption of H_2 and N_2 [103]. On precious metals, N–H cleavage is discussed as the rate-determining step, while for non-precious metals, N_2 desorption is the rate-limiting step. All modifications of the support or the presence of additives may alter the desorption step of N_2 and change therewith the catalytic properties of the catalyst system.

However, even though Ru-based catalysts are most promising for ammonia decomposition, high costs and limited resources of precious metals require the development of more economical alternatives as catalysts. As alternative catalysts mainly Fe, Ni [128,129], Co, or Mo have been investigated, either as pure phases or supported on carbon materials or porous/non-porous oxides. Depending on reaction temperatures, Fe and Mo form different types of nitrides during decomposition, while Co reduces to metallic state which was evidenced by *in situ* diffraction studies [130–133]. Recently, reaction pathways of Mn catalysts (Mn nitrides) were studied by *in situ* neutron diffraction [134].

Iron nanoparticles encapsulated into shells of porous silica are considerably more active in ammonia decomposition than unsupported nanoparticles. The encapsulated catalyst is much more stable since mainly sintering of particles is prevented even at higher temperatures [135,136]. Core–shell nanostructures with SiO_2, Al_2O_3, MgO as porous shell materials and encapsulated catalysts, such as Fe, Co, Ni, and Ru, are interesting but complicated model systems. They may assist with understanding fundamental processes, but compared to pure metals or simple supported catalysts their reaction temperatures are not significantly lower and such systems may not be feasible for large scale industrial applications/production.

In addition to transition metal nitrides, carbides could also be interesting catalysts. The activity of WC and VC for hydrogen generation was investigated by several groups and some interesting properties were reported [137–139].

Metal amide/imide catalysts

Group I and II metal salts have rarely been considered as candidates for ammonia decomposition catalysts outside of their established use as promoters in transition metal systems. However, the catalytic activity of a Group I metal amide was first reported in 1894 by Titherley, who observed continuous decomposition of ammonia by sodium amide ($NaNH_2$) heated to "dull redness" [140]. Titherley proposed that the decomposition was as a result of the concurrent decomposition and synthesis of sodium amide, two reactions which had been observed in isolation:

$$NaNH_2 \rightarrow Na + \tfrac{1}{2} N_2 + H_2$$

$$Na + NH_3 \rightarrow NaNH_2 + \tfrac{1}{2} H_2$$

Despite this observation and the extensive recent interest in light metal amides for solid state hydrogen storage applications [2,141–143], no further investigations of the ammonia decomposition activity of sodium amide were reported until 2014, when a more detailed study found that it showed similar performance to 5% Ru on Al_2O_3 above 425 °C

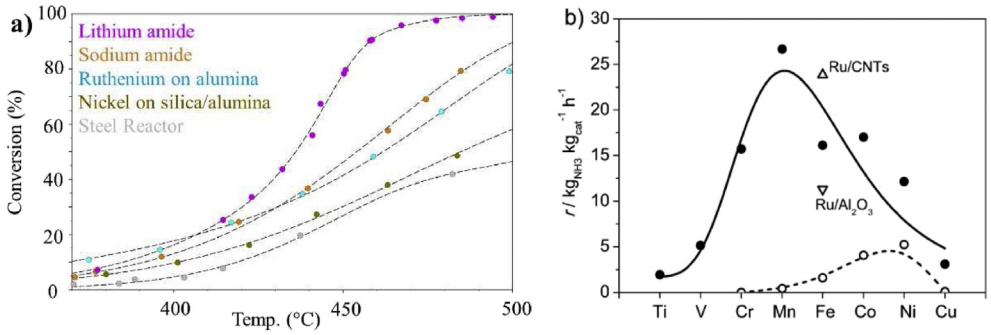

Fig. 5 – Variable-temperature ammonia decomposition performance of a) lithium and sodium amide compared with supported nickel and ruthenium catalysts, measured in a 46.9 cm^3 cylindrical stainless steel reactor (0.5 g catalyst, 60 sccm NH_3 flow), modified with permission from [146]. Copyright 2015 Royal Society of Chemistry; b) lithium imide-transition metal (nitride) composites (filled points) compared with transition metal nitrides (Cr, Mn, Fe) and carbon nanotube supported transition metals (Co, Ni, Cu) (open points), along with selected Ru-based catalysts, reproduced with permission from [145]. Copyright 2015 Wiley-VCH.

[144]. Parallel investigations focused on the synergy of lithium imide (Li_2NH) and 3d transition metals were published later by Chen et al., in 2015 [145].

These results, together with the limitations on the practical use of sodium amide due to its high volatility under operating conditions [140,144], prompted a wider survey of light metal amides and imides for active catalysts. Publications to date have included lithium amide/imide ($LiNH_2/Li_2NH$) [146], lithium imide-3d transition metal composites [145,147], sodium/potassium amide (Na/KNH_2)-manganese nitride [148], lithium-calcium imide ($Li_2Ca(NH)_2$) [149], ruthenium-magnesium/calcium/barium amide ($M(NH_2)_2$, M = Mg, Ca, Ba) [150] and potassium/rubidium-manganese amide ($M_2[Mn(NH_2)_4]$, M = K, Rb) [151]. Of the systems studies thus far, lithium amide/imide-containing materials appear to be the most active, showing significantly superior catalytic activity to 5% Ru on Al_2O_3 [145,146] (Fig. 5a), and superior performance to carbon nanotube-supported ruthenium [145,147], which is widely seen as one of the most active ammonia decomposition catalyst formulations. These results, shown in Fig. 5b, contrast with the accepted promoter activity trends for other alkali metal salts [152], which places lithium as the least active promoter [101].

This activity trend for metal amides points to a different function compared with catalyst promoters. There have been a number of hypotheses as to the precise role of the metal amide/imide in the reaction (Fig. 6). Of particular interest is whether the amide/imide alone can catalyze the decomposition of ammonia. Many of the published studies report the activity of composites of metal amides/imides with transition metals and transition metal nitrides [145,147,148,150,153,154]. In these cases, it is proposed that the catalytic activity results exclusively from the interaction of the amide/imide with the transition metal, either via the ammonia-mediated formation and decomposition of a ternary nitride (e.g. Li_7MnN_4, Li_3FeN_2, Ca_6MnN_5) if possible (Fig. 6iii) [145,147,155], or else by electronic interaction between the metal and NH_x species in the metal amide/imide promoting the cleavage of N–H bonds (Fig. 6ii) [150,153].

Catalytic activity has also been reported for metal amides/imides without the formation of transition metal composites [144,146,149]. For lithium amide-imide, the onset of ammonia decomposition activity was correlated with destabilization of lithium amide to form lithium imide [146]. Isotope studies of the reaction were used to suggest an ammonia decomposition pathway based on the cyclic formation and decomposition of a lithium-rich material such as lithium nitride-hydride (Li_4NH, Fig. 6i) [146]. *In situ* powder diffraction studies have identified solid solutions of lithium amide and imide ($Li_{1+x}NH_{2-x}$,

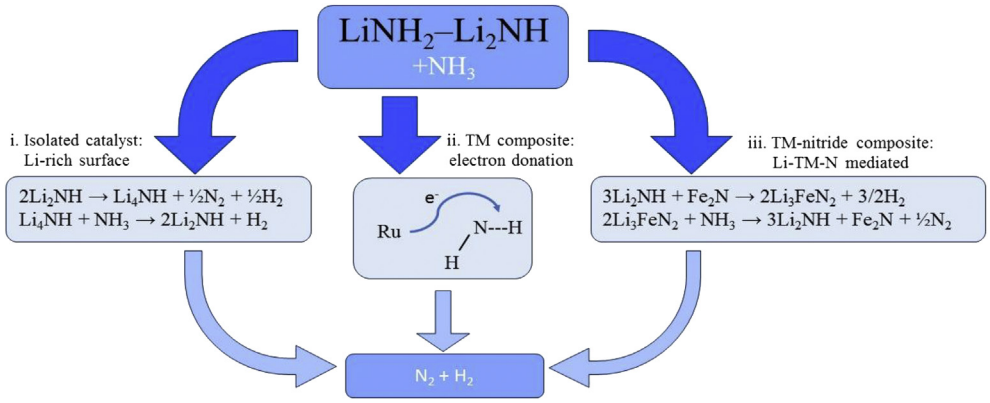

Fig. 6 – Proposed mechanisms for ammonia decomposition reactions involving lithium amide-lithium imide.

$0 < x < 1$) as a bulk phase present under ammonia decomposition conditions (>500 °C under low flow of ammonia) for a number of lithium imide-based catalyst formulations [146,149]. Both lithium nitride-hydride [156] and many ternary lithium nitrides [157,158] are expected to be unstable under ammonia/hydrogen, so it is more likely these species may be observed on the surface or interfaces of catalysts than in the bulk structure.

The studies of isolated metal amides and imides were performed in stainless steel reactors because of concerns over the reactivity of strong basic NH_2^- and NH^{2-} anions with conventional quartz or glass reactors [140,159]. However, the use of stainless steel makes it difficult to rule out the effect of the reactor walls on the catalysis in these studies. Strong evidence exists for the integral involvement of the metal amide/imide in the ammonia decomposition reaction (particularly given the activity observed in combination with otherwise inactive metals such as V and Cr [145]), and for the enhanced ammonia decomposition activity of metal amides and imides combined with transition metals and their nitrides; whether this combination is necessary for catalysis to occur remains an ongoing subject of investigation. In either case, it is clear that there is scope for significant development of this new family of ammonia decomposition catalysts, which use abundant materials to produce hydrogen from ammonia with very high catalytic activity.

Across all ammonia decomposition catalyst systems, further systematic investigations are required to ensure comparable experimental conditions for all materials. This is mandatory to guarantee comparable and sound results. Furthermore, *in situ*/operando studies have shown great potential for a better understanding of catalytic ammonia decomposition and future research will benefit substantially from further experiments in these areas.

Solid-state ammonia storage

Although it is less flammable than hydrogen, ammonia does have significant toxicity concerns, both to humans and, particularly, to marine organisms. While some studies have suggested that ammonia would pose similar risks to existing transportation fuels [160,161], it is clear that advanced controls may be necessary for the use of ammonia in energy infrastructure, both for stationary storage solutions and for applications in the transportation sector, e.g., for automotive deNOx in diesel exhaust. In both cases, cost and safety aspects are essential, while the density of accessible ammonia which can be stored and released close to the operating temperatures is crucial in the latter case.

Storage of ammonia in solids has been considered as a means for safely storing ammonia, offering significantly reduced ammonia vapor pressure [83,91,162]. While this adds a requirement to thermally desorb ammonia from these materials, many such compounds achieve very high volumetric ammonia density (Fig. 7) when compacted into solid tablets [83], and so do not significantly compromise the storage advantages of ammonia. Much of the research on these systems has focused on the relationship between structure, the identity of the metal cation/s and the resultant thermal stability of the ammoniate. Some of the recent work in this area is summarized below.

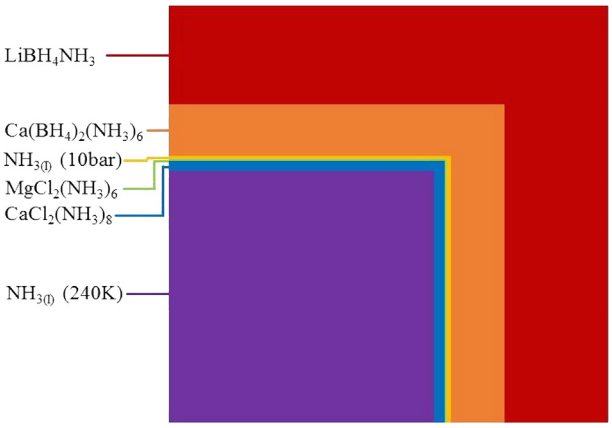

Fig. 7 – Storage volume for a range of different ammonia storage methods, with a constant mass of ammonia. Solids are assumed to be able to be pelletised to 95% of their crystal structure volume [83].

Metal halide ammines

One class of materials which offer a potential solution are metal halide salts such as $MgCl_2$, which can reversibly store 9.1 wt% hydrogen (material-only) in the form of ammonia in $Mg(NH_3)_6Cl_2$ [162]; albeit the ab-/desorption temperature for automotive applications can be better matched with other metal halide salts [83,163].

Through combined use of DFT calculations and evolutionary algorithms, it has been possible to computationally design novel metal halide ammines to exactly match a set of required operating conditions and improvements in the accessible storage capacity by >10% have been achieved using a ternary metal halide [84,164]. These accelerated design strategies are now implemented in the open source Atomic Simulation Environment (ASE) [165] and can be used to design mixed metal halide salts for specific storage solutions by adapting the fitness function of the genetic algorithm to match a specific constrain on, e.g., cost or energy density, yielding excellent agreement with experimental observations [166].

In the design of new metal halide ammines for practical application of the storage materials, both the surface [167] and bulk [168] ab-/desorption kinetics of ammonia should be taken into consideration, as should changes in the crystal structures during ammonia ab-/desorption [169,170], as these may lead to large stresses on the storage containers.

Ammine metal borohydrides

One recently-explored alternative to metal halide ammoniates are ammine metal borohydrides. More than 45 ammonia metal borohydrides have been synthesised and characterised in the past few years and they represent a range of different structure types [171,172]. Metal borohydrides, which themselves have been extensively investigated as hydrogen storage materials [6,8,172] often form 3D framework structures where BH_4^- complexes bridge two metal atoms by edge sharing (η^2), e.g. the structures of magnesium, calcium, strontium, manganese and yttrium borohydride where the metals form tetrahedra, $[M(BH_4)_4]$, or octahedra, $[M(BH_4)_6]$ [173]. Introduction of NH_3

molecules interrupts these frameworks; the ammine yttrium borohydrides, $Y(BH_4)_3 \cdot nNH_3$ are an illustrative example [174]. With one ammonia molecule in the formula unit, n = 1, the structure consists of two-dimensional layers, while with n = 2, the structure is chain-like, 1D. With n = 4 and 5 the structure is built from neutral molecular complexes, and with n = 6 and 7 from complex cations, $[Y(NH_3)_n]^{3+}$ with BH_4^- complexes as counter ion in the solids [174].

In these compounds the BH_4^- complex contributes significantly to the structural diversity of ammine metal borohydrides. The BH_4^- tetrahedra coordinate to a metal in a flexible manner with a range of M – B distances and varying hapticities from η^0 to η^3, i.e. BH_4^- can be either terminal or bridging ligand or act as a counter ion in the solid state [171,173]. This contrasts the ammonia molecule that coordinates more strongly with less flexibility, always via the electron pair donated by nitrogen, and acts as a terminal ligand [172].

Comparison of ammine metal borohydrides and ammine metal halides. Structural analogies between ammine metal borohydrides and chlorides/bromides exist, considering only heavier atoms, i.e. neglecting hydrogen atoms. For example, $M(BH_4)_2 \cdot 6NH_3$ (M = Mg, Mn and Ca) and $MgX_2 \cdot 6NH_3$ (X = Cl and Br) are isostructural [175,176], and $Sr(BH_4)_2 \cdot 2NH_3$ and $MCl_2 \cdot 2NH_3$ (M = Ca and Sr) are structurally similar [177]. The borohydride complex, BH_4^-, is a non-spherical anion in contrast to the halide anions; therefore crystal structures of ammine metal borohydrides often have lower symmetry than their halide analogues, as usually observed when comparing metal borohydrides and metal halides [171]. The structural similarities are most pronounced for compounds with higher number of coordinated ammonia molecules (n), where both BH_4^- and the halides X^-, anions act as counter ions in the solid-state with a predominantly ionic bonding, η^0. Significant structural differences of $MgX_2 \cdot nNH_3$, X = BH_4^- or halides, are observed for smaller number of NH_3 ligands (low n) due to the presence of di-hydrogen bonds and the non-spherical shape of BH_4^-.

Despite minor differences, the thermal stability for ammine metal borohydrides and chlorides are similar when comparing the peak temperature of NH_3 release, e.g. $Y(BH_4)_3 \cdot 7NH_3$ (~80 °C) and $YCl_3 \cdot 7NH_3$ (~100 °C), and $Mg(BH_4)_2 \cdot 6NH_3$ and $MgCl_2 \cdot 6NH_3$ have similar stability (~150 °C), whereas $Mn(BH_4)_2 \cdot 6NH_3$ (~130 °C) is slightly more stable than $MnCl_2 \cdot 6NH_3$ (~105 °C).

Di-hydrogen bonds in the structures. All ammine metal borohydride structures contain di-hydrogen $H^{\delta-} \ldots H^{\delta+}$ contacts between partly positively charged hydrogen, $H^{\delta+}$ bonded to N in NH_3 and partly negatively charged hydrogen, $H^{\delta-}$ bonded to B in BH_4^-. For $Y(BH_4)_3 \cdot nNH_3$ and $Sr(BH_4)_2 \cdot 4NH_3$ the shortest di-hydrogen contacts are in the range 1.850–2.035 Å and are intermolecular, either connecting layers, chains, molecular clusters or connecting complex ions, while it is intramolecular for $Sr(BH_4)_2 \cdot nNH_3$ (n = 1 and 2) within a 2D layer [174,177]. In comparison, the intramolecular hydrogen contacts between $H^{\delta-} \cdots H^{\delta-}$ in a BH_4^- complexes and $H^{\delta+} \cdots H^{\delta+}$ in NH_3 molecules are ~2.00 Å and 1.63 Å, respectively, while the shortest di-hydrogen contact in NH_3BH_3 is 2.02 Å.

Trends in thermal decomposition. The thermal decomposition of a large number of ammine metal borohydrides has been investigated and revealed that ammonia absorption results in the destabilization of metal borohydrides with low electronegativity metals (χ_p < 1.6), while metal borohydrides with high electronegativity metals (χ_p > 1.6) are stabilized by NH_3. The stabilization is possibly due to shielding of metals with high electronegativity by complex formation.

A characteristic of the ammine metal borohydrides which does not occur for metal halides is the potential for gas release either as hydrogen or ammonia. Tailoring which gas is released could be useful in employing ammine metal borohydrides in particular applications, especially as ammonia must often be decomposed before use. The mechanism for decomposition of ammine metal borohydrides remains not fully understood. Strong di-hydrogen bonds have been hypothesised to cause H_2 elimination in the solid-state. However, detailed analysis of experimental data disagree with this hypothesis. For example, ammonia release is observed for $Y(BH_4)_3 \cdot nNH_3$ (n = 7 and 6), which has the strongest di-hydrogen bonds (~1.85 Å) among the series of compounds, $Y(BH_4)_3 \cdot nNH_3$ (n = 7, 6, 5, 4, 2 and 1) [174]. Similarly, $NaBH_4 \cdot 2H_2O$ does not directly release H_2, but decomposes into $NaBH_4$ dissolved in the crystal water, despite the presence of strong di-hydrogen bonds (1.77–1.95 Å) [178].

The NH_3/BH_4^- ratio (n/m) has also been suggested as an important factor in determining the composition of the released gas. The ratio (n/m) has been adjusted for the series of $M(BH_4)_m \cdot nNH_3$ (M = Mg, Mn and Y), leading to increased H_2 content for lower n/m ratios. However, despite low n/m ratios, $LiBH_4 \cdot NH_3$, $Ca(BH_4)_2 \cdot NH_3$ and $Sr(BH_4)_2 \cdot NH_3$ release NH_3, and not H_2.

Alternatively, two other factors have also been suggested that the composition of the released gasses [177]:

(i) The stability of the metal borohydride (Fig. 8). Ammine metal borohydrides of relatively stable metal borohydrides (χp < ~1.0), e.g. $LiBH_4 \cdot NH_3$, $Ca(BH_4)_2 \cdot nNH_3$ and $Sr(BH_4)_2 \cdot nNH_3$ [177], release NH_3 (with no H_2) by thermolysis in open systems and/or in a flow of an inert gas, i.e. p (NH_3) ~ 0, even when the NH_3/BH_4^- ratios (n/m) are low, ≤1. This may be due to the significantly higher thermal stability of the respective metal borohydrides [177].

Ammine metal borohydrides of less stable metal borohydrides, Al, Zn, or Zr release NH_3/H_2 gas mixtures, which may be due to the lower decomposition temperature of the respective metal borohydrides. Thus, the less stable metal borohydrides react with NH_3 upon decomposition and release H_2 (and in some cases also some NH_3). As an example, $Al(BH_4)_3 \cdot 6NH_3$ releases H_2 and small amount of NH_3 at ~165 °C, and $Al(BH_4)_3$ decompose at significantly lower temperatures, T_{dec} ($Al(BH_4)_3$) ~ 25 °C [10]. $Zn(BH_4)_2 \cdot 2NH_3$ releases 8.9 wt% H_2 at T < 115 °C in contrast to $LiZn_2(BH_4)_5$, which releases a mixture of diborane and hydrogen via reduction of Zn^{2+} to Zn [179,180].

(ii) The partial pressure of ammonia during decomposition. In a closed system, the partial pressure of ammonia is increasing upon ammonia release, p (NH_3) > 0. Then, $LiBH_4 \cdot NH_3$, $Ca(BH_4)_2 \cdot nNH_3$ and $Sr(BH_4)_2 \cdot nNH_3$ first release some ammonia but release hydrogen exothermically at higher

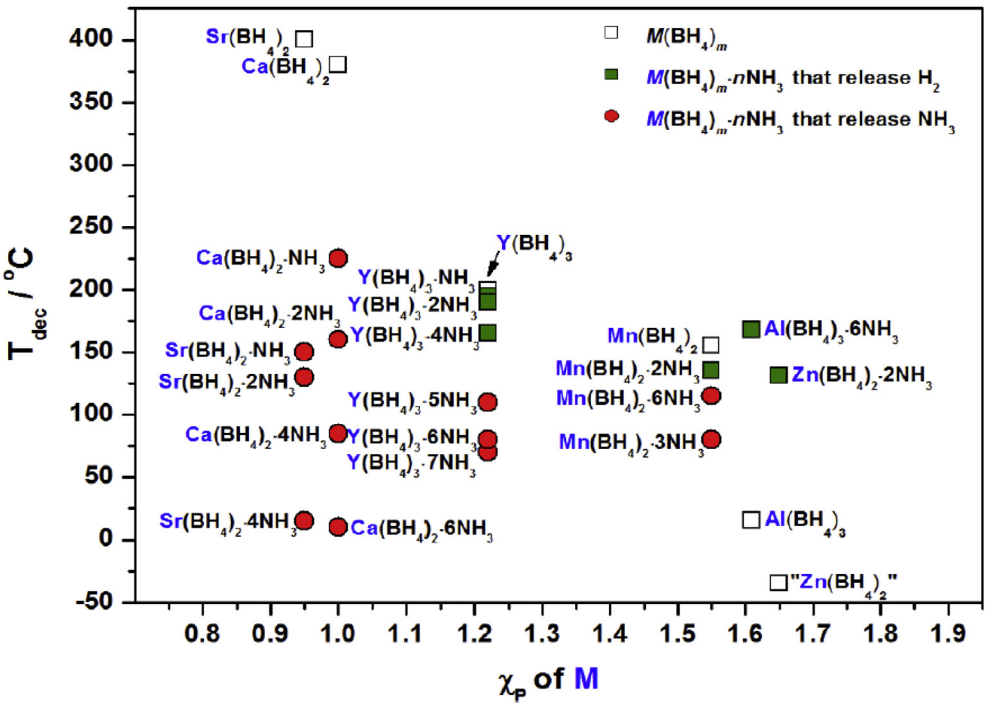

Fig. 8 – Decomposition temperatures, T_{dec}, for selected ammine metal borohydrides and the corresponding metal borohydrides. $Zn(BH_4)_2$ is not experimentally observed and is considered unstable. Reprinted with permission from [177]. Copyright 2015 Wiley-VCH.

temperatures, possibly via a solid-gas hydrogen elimination reaction between solid metal borohydrides and ammonia gas. Thus, when the ammonia release temperature of ammine metal borohydrides is significantly lower than the decomposition temperature of the corresponding metal borohydride, then initially ammonia is released, which react with the metal borohydride at higher temperatures via solid-gas reactions, when confined in a closed systems [177].

Using these characteristics governing the desorbed gas composition from ammine metal borohydrides as design rules may help develop systems with tailored gas compositions, generating the various levels of ammonia decomposition needed for different applications (Fig. 4).

Sorbent and membrane approaches to ammonia removal

Ammonia has been demonstrated to be irreversibly damaging to PEM fuel cells at low-ppm concentration levels [181,182]. While advances in ammonia decomposition catalysts will significantly assist in producing high-purity ammonia, reaching the <0.1 ppm benchmark for PEM fuel cells is beyond the thermodynamic limit for temperatures less than 725 °C, as shown in Fig. 9. Ammonia emissions must also be avoided even in the case of ammonia-tolerant power generation systems (e.g. alkaline fuel cells [183]) because of the toxicity of ammonia. As such, if ammonia is to be used as a hydrogen carrier, approaches to remove residual ammonia from the hydrogen gas stream are required.

Sorbent materials have been proposed as a means to achieve ultra-low concentrations of ammonia in dynamic hydrogen gas streams. Recently, lithium exchange type X zeolite was used in a flow of simulated cracked ammonia (1000 ppm inlet concentration) to give 0.01–0.02 ppm ammonia in the purified hydrogen/nitrogen stream, up to a maximum storage capacity of 5.7 wt% [185]. Similar studies have also been reported for a number of metal halide sorbent systems, reaching storage capacities in excess of 10 wt% [186].

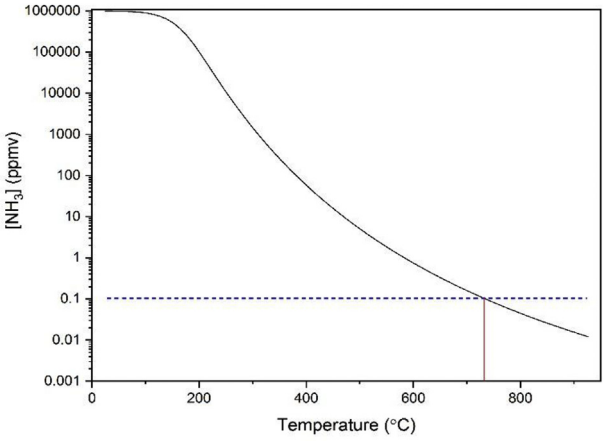

Fig. 9 – Variable-temperature equilibrium ammonia concentration at 0.1 MPa. The acceptable level for PEM fuel cells is shown as a dashed blue line, with the corresponding equilibrium temperature indicated with a red line. Thermodynamic data calculated from variable-temperature heat capacity data from Ref. [184]. (For interpretation of the references to colour in this figure legend, the reader is referred to the Web version of this article.)

Sorbent-based approaches such as these would function on the use of a cartridge of sorbent which could be regenerated by the application of heat to drive off the adsorbed ammonia.

There have also been recent advances in the use of membranes to purify hydrogen from cracked ammonia. A recently developed layered palladium-vanadium membrane offers significant cost benefit over pure palladium membranes [187,188]; while fragile membranes may not yet be suitable for on-board hydrogen purification, they are strong candidates for use in the production of pure hydrogen from cracked ammonia at the forecourt or in centralised facilities. A key advantage of membrane-based approaches is the simultaneous removal of nitrogen from the gas stream, avoiding the need for the use of pressure-swing adsorption or other secondary purification techniques.

Reversible liquid organic hydrogen carriers (LOHCs)

In the present review, formic acid and methanol as organic hydrogen carriers are not included. Therefore, in the LOHCs part, we only discuss cycloalkanes and their derivatives, such as N-heterocycles, substituted alkanes and fused ring compounds *etc.* LOHCs with hydrogen content of ~5–8 wt%, reversibility, moderate dehydrogenation temperature, commercial availability, production of CO_x-free hydrogen and more importantly, the compatibility with existing gasoline infrastructure, hold the promises as hydrogen carriers for both onboard application and large-scale, long-distance H_2 transportation [41,189–191]. However, the cycloalkanes, such as cyclohexane, methylcyclohexane and decalin, usually suffer from their high dehydrogenation enthalpy changes, requiring high dehydrogenation temperature [192]. Therefore, the development of new materials with favorable dehydrogenation enthalpy change (ΔH_d) is needed. On the other hand, kinetic barriers exist in both dehydrogenation and hydrogenation processes, which need optimization on catalysts. Therefore, the recent advances in these two aspects (thermodynamic and kinetic optimizations) will be summarized and discussed in the present review.

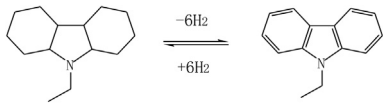

Scheme 1 – Dehydrogenation and hydrogenation of 12H-NEC and NEC pair.

Thermodynamic optimization

Early research on liquid organic hydrides for hydrogen storage focused on cyclohexane-benzene pair, methylcyclohexane-toluene pair, and decalin-naphthalene pair [192]. However, the dehydrogenation of these cycloalkanes occurs at relatively high temperature (usually higher than 300 °C) due to their high dehydrogenation enthalpy changes. Taking methylcyclohexane as an example, the calculated dehydrogenation enthalpy change is around 73.6 kJ mol^{-1} H_2, leading to a dehydrogenation temperature of *ca.* 326 °C [193]. The strategies for optimization of ΔH_d from literature, including fused ring compound, heteroatom replacement and electron-donating substitution, are summarized in Fig. 10. It is shown that the decalin-naphthalene pair exhibits lower enthalpy change during dehydrogenation, hinting that the fused ring strategy is an optional method to optimize the thermodynamic properties [41]. Pez. et al. from Air Products and Chemicals company had predicted theoretically and demonstrated experimentally in their patent that fused ring compounds possess lower dehydrogenation enthalpy changes [194], in which the hydrogen storage properties of several fused ring compounds including pyrene, coronene and hexabenzocoronene were tested, showing superb reversible hydrogen storage properties compared with that of mono-ring counterpart (benzene-cyclohexane pair).

In the following patent from Air Products and Chemicals [190], it was demonstrated that better reversible hydrogen storage properties can be obtained by using heteroatoms (such as N, O, P, or B etc.) substituted hydrocarbons. Particularly, the dehydrogenation enthalpy changes are effectively enhanced in the N-heterocycles (Fig. 10), among which the N-ethylcarbazole (NEC) and dodecahydro-N-ethylcarbazole

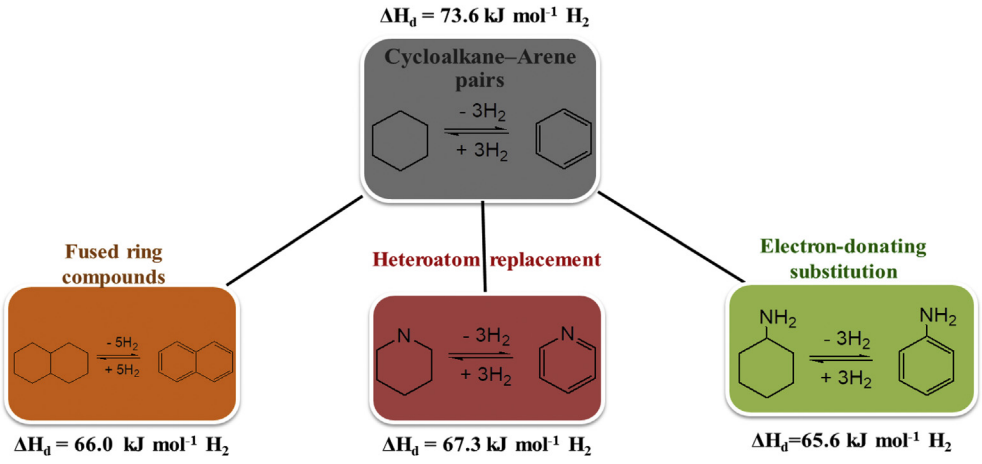

Fig. 10 – Strategies for optimization of dehydrogenation enthalpy change of cycloalkane in the literature.

(12H-NEC) pair with ΔH_d of 50.6 kJ mol^{-1} H_2 exhibits superior reversible de/hydrogenation properties as shown in Scheme 1. 12H-NEC is liquid at room temperature and has a theoretical material gravimetric capacity of 5.8 wt%, exhibiting a potential candidate for liquid phase hydrogen storage application. As such, much attention has been given to the reversible NEC and 12H-NEC pair, especially in catalyst development which will be introduced in the following sections. Independently, Clot, Eisenstein and Crabtree et al. calculated the thermodynamic data and theoretical dehydrogenation temperature under 1 bar hydrogen of a series of N-heterocycles and found that the dehydrogenation enthalpy change can be effectively reduced by incorporation of N atoms into the rings [193], which may be due to that the N substituents can weaken α-CH bond in a saturated species. Actually, *in situ* XPS and *in situ* FTIR studies on the dehydrogenation of 12H-NEC indicated that the dehydrogenation started from the five-membered ring by weakening the C–H bond adjacent to N atom on Pd– and Pt-based model catalysts [195–197].

The calculation from Crabtree et al. also revealed that the substituted N outside the ring can be even more effective than a ring N in lowering ΔH_d through comparison of benzene-cyclohexane (ΔH_d = 17.6 kcal $mol^{-1}H_2$), pyrideine-piperidine (ΔH_d = 16.1 kcal mol^{-1} H_2) and aniline-cyclohexylamine (ΔH_d = 15.7 kcal mol^{-1} H_2) [193], which means the addition of electron donating groups would lower the temperature at which hydrogen can be easily released. Jessop and coworkers found a correlation between the dehydrogenation enthalpy of cycloalkane and Hammett parameter (σ) of substitute group as shown in Fig. 11 [198]. The Hammett parameter reflects electron donating ability of substituent group. Their work showed a linear correlation, *i.e.*, the lower the Hammett parameter (or the more electron-donating substituent) the lower dehydrogenation enthalpy. Therefore, the electron-donating strategy would be a promising way to optimize the thermodynamic properties. However, the substituents outside the ring would have the chance to detach from the parent substance under harsh condition during dehydrogenation [198].

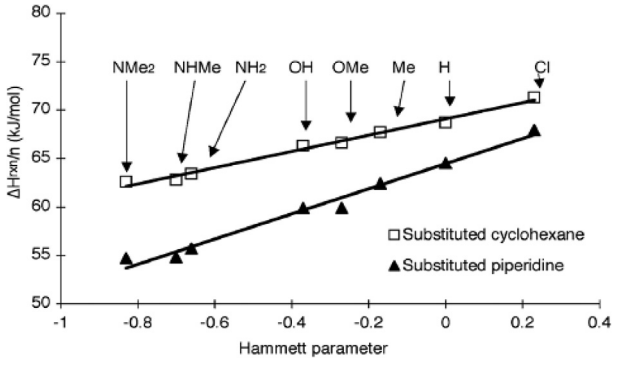

Fig. 11 – Calculated dehydrogenation enthalpies ($\Delta H_{rxn}/n$) of mono-substituted cyclohexane and para-substituted piperidine derivatives. Reprinted with permission from [198]. Copyright 2008 Royal Society of Chemistry.

Kinetic optimization

Heterogeneous catalysts

Since the N-heterocycles exhibit reduced dehydrogenation enthalpy changes, much attention has been given to these systems, especially on the development of catalysts. Crabtree and coworkers investigated several noble catalysts (Pd, Rh *etc.*) for the dehydrogenation of indoline and achieved 100% conversion using Pd/C catalyst only after half an hour in refluxing toluene [199]. For the heterogeneous catalyst, support is one of the key factors to the activity and stability. Sánchez-Delgado found that the hydrogenation rate of quinoline increased monotonically with the basicity of the support, *i.e.*, MgO < CaO < SrO [200,201]. Therefore, they proposed mechanism for catalytic hydrogenation, which involved the heterolytic hydrogen splitting and ionic hydrogenation on the metal/basic support interface due to the polarity of C=N bond in quinoline [201,202]. By using this heterolytic hydrogen splitting function of the basic support, covalent triazine framework (CTF, a microporous support) supported Pd nanoparticles exhibited an improved activity in the hydrogenation of N-heterocycles in comparison with active carbon support [203]. Recently, Somorjai et al. used dendrimer-stabilized noble metal nanoparticles for the dehydrogenation/hydrogenation of N-heterocycles (tetrahydroquinoline and indoline) and achieved reversible hydrogen release and storage under mild condition, *i.e.*, 130 °C and 60 °C for dehydrogenation and hydrogenation, respectively, which may be attributed to the basic property of the dendrimer support [204].

Unfortunately, only the N-heterocyclic parts participated in the dehydrogenation/hydrogenation in the above examples, meaning quite low usable hydrogen contents. As mentioned above, NEC and 12H-NEC pair with suitable thermodynamic properties and high hydrogen capacity (5.8 wt%) has drawn tremendous effort in the past decade. Table 2 summaries the recent development of heterogeneous catalyst for this pair. The reversible NEC and 12H-NEC pair for hydrogen storage was firstly proposed by Air Products [190,194]. From the literature, it was found that Ru is the most active catalyst for hydrogenation [205,206]. Pd, on the other hand, appears to be highly active for dehydrogenation [207–209]. In the Air Products' patents, Ru and Pd on lithium aluminate were employed as hydrogenation and dehydrogenation catalysts, respectively [190], where *ca.* 5.6 wt% hydrogen can be reversibly stored and released. Smith and coworkers found around 100% conversion at 170 °C over 5% Pd/SiO_2 catalyst for 12H-NEC dehydrogenation [205], showing outstanding catalytic capability. However, the partially dehydrogenated intermediates, such as octa- and teterahydro-N-ethylcarbazole (8H-NEC and 4H-NEC), were found in the products. Similarly, Cheng et al. investigated the reversible hydrogen storage properties of NEC and 12H-NEC pair and found that the full hydrogenation of NEC was realized over a 5% Ru/Al_2O_3 catalyst at 180 °C and 8.0 MPa hydrogen [210]. However, the dehydrogenation underwent a three stage process with a 5%Pd/Al_2O_3 catalyst, *i.e.*, from 12H-NEC to 8H-NEC to 4H-NEC and further to NEC with the initial reaction temperatures of 128 °C, 145 °C, and 178 °C, respectively. Smith and coworkers found the dehydrogenation activity and selectivity

Table 2 – Heterogeneous catalysts for dehydrogenation/hydrogenation of NEC and 12H-NEC pair.

Catalysts	De/hydrogenation	Temperature /pressure	Products	Solvents	Refs.
5%Ru/lithium aluminate	Hydrogenation	160 °C/6.9 MPa	12-NEC	–	[190]
4%Pd/lithium aluminate	Dehydrogenation	197 °C/0.1 MPa	NEC	–	[190]
5%Ru/Al_2O_3	Hydrogenation	130–150 °C/7 MPa	>95% 12-NEC	decalin	[205]
5% Pd/SiO_2	Dehydrogenation	150–170 °C/-	NEC, 4H-NEC, 8H-NEC	decalin	[205]
5% Pd/C	Dehydrogenation	170 °C/-	NEC	decalin	[207]
4%Pd/SiO_2(9 nm)	Dehydrogenation	170 °C/-	NEC	decalin	[208,209]
Ru black	Hydrogenation	130 °C/7 MPa	12H-NEC, 8H-NEC, 4H-NEC	cyclohexane	[211]
Pd black	Hydrogenation	130 °C/7 MPa	12H-NEC, 4H-NEC	cyclohexane	[211]
Pt black	Hydrogenation	130 °C/7 MPa	12H-NEC, NEC	cyclohexane	[211]
65%Ni/SiO_2–Al_2O_3	Hydrogenation	130 °C/7 MPa	12H-NEC, NEC	cyclohexane	[211]
5%Ru/Al_2O_3	Hydrogenation	130 °C/7 MPa	98% 12H-NEC	molten reaction mixture	[212]
5% Ru/TiO_2	Hydrogenation	130 °C/7 MPa	12H-NEC, 8H-NEC, 4H-NEC	cyclohexane	[213]
5t% Ru/Al_2O_3	Hydrogenation	130 °C/7 MPa	12H-NEC, 8H-NEC, 4H-NEC	cyclohexane	[213]
Ru black	Hydrogenation	130 °C/7 MPa	12H-NEC, 8H-NEC, 4H-NEC	cyclohexane	[213]
Ru black	Hydrogenation	130 °C/7 MPa	12H-NEC, 8H-NEC, 4H-NEC	1,4-dioxane	[214]
Ru–, Rh–, Pd-based catalysts	Hydrogenation	130 °C/7 MPa	12H-NEC, 8H-NEC, 4H-NEC	cyclohexane	[206]
5%Ru/Al_2O_3	Hydrogenation	180 °C/8 MPa	12H-NEC,	–	[210]
5%Pd/Al_2O_3	Dehydrogenation	128 °C,145 °C,178 °C/-	8H-NEC, 4H-NEC, NEC	–	[210]

were strongly dependent upon the Pd size, *i.e.*, the maxima in both activity and selectivity were obtained over a Pd/SiO_2 catalyst with an average particle size of 9 nm [208,209]. Although Ru catalyst showed the best activity for the hydrogenation of NEC, it suffered from lower selectivity to the desired product. Rh-based catalysts, on the other hand, exhibit a higher selectivity to 12H-NEC under comparable conditions [206].

Homogeneous catalysts

Catalytic dehydrogenation of 12H-NEC was also reported using homogeneous catalysts. In 2009, Jensen and coworkers found that an Ir-PCP pincer complex was an efficient catalyst for the dehydrogenation of 12H-NEC at 200 °C [215]. Meanwhile, they found that this Ir-based homogeneous catalyst was also active for the other organic hydrogen carriers, including perhydrodibenzofuran, perhydroindole, N-methyl perhydroindole,

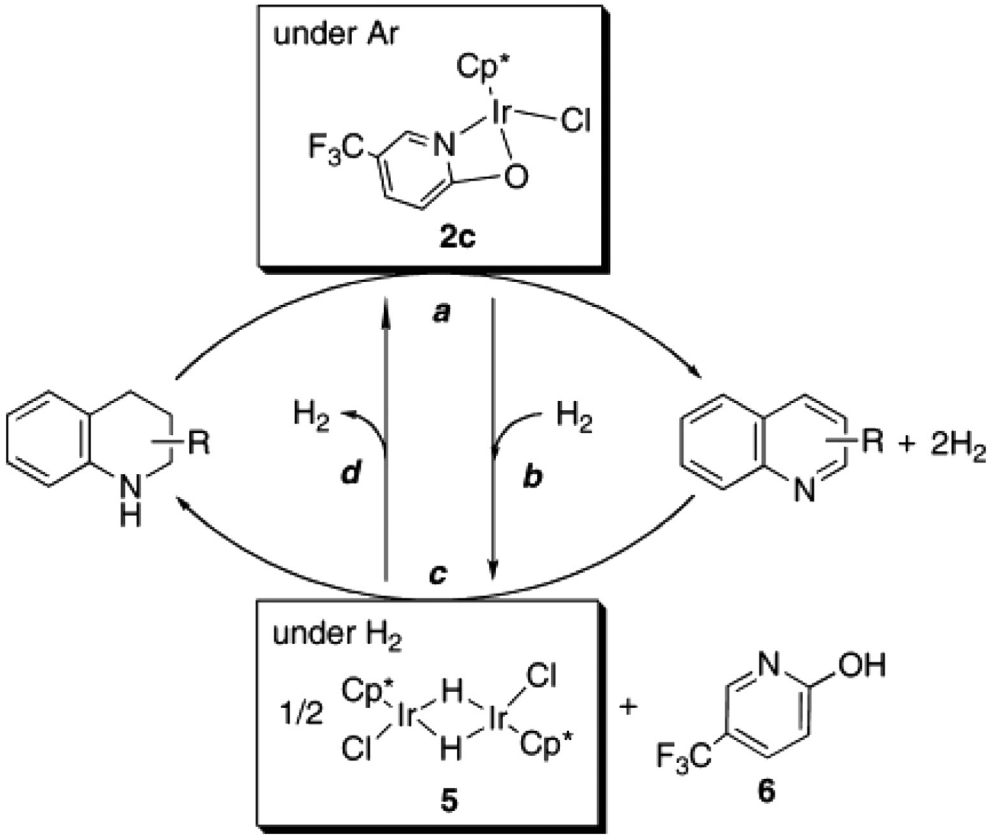

Fig. 12 – Over processes for the reversible catalytic dehydrogenation/hydrogenation of 2-MeTHQ.

etc. [216] Fujita and Yamaguchi also developed a Cp*Ir complex homogeneous catalyst bearing a 2-pyridonate ligand (Cp* = pentamethylcyclophentadienyl) exhibited excellent activity in the reversible dehydrogenation/hydrogenation of 2-methyl-1, 2, 3, 4-tetrahydroquinoline (2Me-THQ) [217]. The author proposed a dehydrogenation/hydrogenation mechanism according to their experiment (Fig. 12). Under hydrogen pressure, the catalyst would convert to a hydride-bridged dinuclear Cp*Ir complex (**5** in Figure 12) that may catalyze the hydrogenation reaction by transfer hydrides to quinoline. However, the hydride would be liberated from the hydride-bridged dinuclear Cp*Ir complex under Ar, forming **2c** in Fig. 12, which would have the ability to catalyze the dehydrogenation of 2Me-THQ. However, only the N-heterocyclic part of the bicyclic quinoline system participates in both transformations and, consequently, the hydrogen gravimetric capacity of this system is quite low. Therefore, in the following investigation, they achieved efficient homogeneous perdehydrogenation of 2,6dimertyldecahydro-1,5-naphthyridine with release and uptake of five molecules of H_2 catalyzed by Cp*Ir complexes bearing functional bipyridonate ligands as a single precatalyst, which increased the hydrogen capacity dramatically [218]. Xiao and coworkers also reported a versatile cyclometalated [Cp^*Ir^{III}]/imino complex for acceptorless dehydrogenation of N-heterocycles [219,220].

Despite the recent progress with Ir-based catalysts [215,217–221], the development of low-cost, non-noble metal catalyst for the dehydrogenation or hydrogenation of N-heterocycles is highly desirable. Jones and coworkers synthesised a (^{iPr}PNP)Fe(CO)(H) bifunctional catalyst (^{iPr}PNP = $^{i}Pr_2PCH2_CH_2NCH_2CH_2P^{i}Pr_2$), which exhibited excellent performance in both dehydrogenation and hydrogenation of N-heterocycles [222]. Theoretical analyses on this Fe catalyst showed that the dehydrogenation mechanism of saturated N-heterocyclic substrates was highly dependent on the polarity of the C–N bond, *i.e.*, the relatively unpolarized C–N bonds are dehydrogenated through a concerted proton/hydride transfer, whereas, the polarized C–N bonds entail stepwise (proton then hydride) bifunctional dehydrogenation [222,223]. Beside this Fe-based catalyst, Co-[224] and Ni-based [225] non-noble homogeneous catalysts were also reported by Jones' group and Crabtree's groups, respectively. Usually, these homogeneous catalysts require more than 20 h reaction time at high temperature. Li and coworker achieved acceptorless dehydrogenation of a series of N-heterocycles at ambient temperature by merging visible-light photoredox catalysis [226], where $Co(dmgH)_2Cl_2$ and Ru $(bpy)_3Cl_2 \cdot 6H_2O$ were employed as catalyst and photosensitizer, respectively. In spite of advances were reported recently, the stability and reusability are main issues for the homogeneous catalysts, which needs further investigation in the future.

Conclusions and future opportunities

Hydrogen is likely to play a key role alongside electrification in decarbonising global energy systems. The high volumetric hydrogen density and ease of storage and transportation make liquid hydrogen-containing carriers attractive for reducing the infrastructure burden of implementing hydrogen-based energy storage. Key opportunities exist already for the use of liquid carriers in facilitating hydrogen trade and inter-seasonal energy storage, with possible extensions towards on-board hydrogen storage for transportation. While much of the required technology to implement these carriers exists already, there are a number of areas where further improvements can be made. Designing lower cost, highly active catalysts which enable high round-trip efficiencies and dehydrogenation at moderate temperatures will always improve the economic viability of energy storage. There are particular opportunities to develop new catalysts which can integrate directly with intermittent renewable electricity generation. Therefore, continuing work in the development of electrocatalysts and catalysts which can operate under more moderate and variable reaction conditions, as well as thermochemical cycles for liquid carrier production, will be central to broadening the application liquid hydrogen carriers.

Acknowledgments

JWM acknowledges St John's College and the John Fell Fund, Oxford, for financial support. TH and PC acknowledge the support provided by the National Natural Science Foundation of China (51671178, 21875246, 51472237), DICP (DICP ZZBS201616), and Sino-Japanese Research Cooperative Program of the Ministry of Science and Technology (2016YFE0118300). CW thanks the Max Planck Society for basic funding. F.C. thanks NWO-Vici (16.130.344) for funding. P.N. and P.E.d.J. acknowledge support from the European Research Council (ERC) under the European Union's Horizon 2020 research and innovation programme (ERC-2014-CoG No 648991). TJ acknowledges the support of the Danish council for independent research, technology and production (DFF – 4181–00462), The Nordic Neutron Science Program, NordForsk (FunHy, project no. 81942) and the Carlsberg Foundation. TV acknowledges support from The Villum Foundation through V-Sustain: The VILLUM Centre for the Science of Sustainable Fuels and Chemicals (#9455). WIFD acknowledges the EPSRC for grant funding (EP/M014371/1). Dr Thomas Wood is thanked for useful discussions. Dr Jianping Guo is thanked for feedback on the ammonia decomposition section.

Author contributions

All authors contributed to the design of the manuscript and commented on draft versions. JWM and WIFD coordinated the planning and writing of the manuscript. JWM and WIFD wrote section Introduction. JWM wrote sections Ammonia, Metal amide/imide catalysts, and Sorbent and membrane approaches to ammonia removal; TH and PC wrote section Reversible liquid organic hydrogen carriers (LOHCs); CW wrote section Transition metal catalysts; PEdJ, FC and PN wrote section Thermal ammonia production; TJ wrote section Ammine metal borohydrides; TV wrote sections Electrochemical ammonia production and Metal halide ammines; YK contributed to section Sorbent and membrane approaches to ammonia removal.

Appendix A. Supplementary data

The research materials supporting this publication can be accessed by contacting the relevant author/s for each of the papers cited in this review.

Supplementary data related to this article can be found at https://doi.org/10.1016/j.ijhydene.2019.01.144.

REFERENCES

[1] Argonne National Laboratory. Basic research needs for the hydrogen economy. 2004.
[2] Gregory DH. Lithium nitrides, imides and amides as lightweight, reversible hydrogen stores. J Mater Chem 2008;18:2321. https://doi.org/10.1039/b801021h.
[3] Wang J, Li H-W, Chen P. Amides and borohydrides for high-capacity solid-state hydrogen storage—materials design and kinetic improvements. MRS Bull 2013;38:480–7. https://doi.org/10.1557/mrs.2013.131.
[4] Suh MP, Park HJ, Prasad TK, Lim D-W. Hydrogen storage in metal-organic frameworks. Chem Rev 2012;112:782–835. https://doi.org/10.1021/cr200274s.
[5] Grochala W, Edwards PP. Thermal decomposition of the non-interstitial hydrides for the storage and production of hydrogen. Chem Rev 2004;104:1283–316. https://doi.org/10.1021/cr030691s.
[6] Huang Z, Autrey T. Boron-nitrogen-hydrogen (BNH) compounds: recent developments in hydrogen storage, applications in hydrogenation and catalysis, and new syntheses. Energy Environ Sci 2012;5:9257. https://doi.org/10.1039/c2ee23039a.
[7] Orimo S-I, Nakamori Y, Eliseo JR, Züttel A, Jensen CM. Complex hydrides for hydrogen storage. Chem Rev 2007;107:4111–32. https://doi.org/10.1021/cr0501846.
[8] Li H-W, Yan Y, Orimo S, Züttel A, Jensen CM. Recent progress in metal borohydrides for hydrogen storage. Energies 2011;4:185–214. https://doi.org/10.3390/en4010185.
[9] David WIF. Effective hydrogen storage: a strategic chemistry challenge. Faraday Discuss 2011;151:399. https://doi.org/10.1039/c1fd00105a.
[10] Møller KT, Sheppard D, Ravnsbæk DB, Buckley CE, Akiba E, Li H, et al. Complex metal hydrides for hydrogen , thermal and electrochemical energy storage. Energies 2017;10:1645. https://doi.org/10.3390/en10101645.
[11] von Helmolt R, Eberle U. Fuel cell vehicles: Status 2007. J Power Sources 2007;165:833–43. https://doi.org/10.1016/j.jpowsour.2006.12.073.
[12] Toyota Motor Corporation. Mirai fuel cell vehicle. 2017.
[13] Honda. Honda clarity fuel cell press kit 2017. 2017. accessed, https://hondanews.eu/eu/en/cars/media/pressreleases/106336/2017-honda-clarity-fuel-cell-press-kit (Accessed 8 August 2018).
[14] Hyundai. Hyundai ix35 hydrogen fuel cell vehicle n.d. https://www.hyundai.co.uk/about-us/environment/hydrogen-fuel-cell (Accessed August 8, 2018).
[15] Audi. Audi h-tron quattro concept n.d. https://www.audi.com/en/innovation/futuredrive/h-tron_quattro.html (Accessed August 8, 2018).
[16] Mercedes-Benz. The new GLC F-CELL n.d. https://www.mercedes-benz.com/en/mercedes-benz/vehicles/passenger-cars/glc/the-new-glc-f-cell/ (Accessed August 8, 2018).
[17] Riversimple. Our partners and collaborators. 2018. https://www.riversimple.com/our-partners-and-collaborators/ (Accessed 8 August 2018).
[18] U.S. Department of Energy: Office of Energy Efficiency & Renewable Energy. DOE technical targets for onboard hydrogen storage for light-duty vehicles n.d. https://www.energy.gov/eere/fuelcells/doe-technical-targets-onboard-hydrogen-storage-light-duty-vehicles (Accessed August 8, 2018).
[19] ACIL Allen Consulting. Opportunities for Australia from hydrogen exports. 2018.
[20] Imperial College London. Analysis of alternative UK heat decarbonisation pathways. 2018.
[21] U.S. Department of Labor: Occupational safety and Health administration. OSHA Annotated Table Z-1 n.d. https://www.osha.gov/dsg/annotated-pels/tablez-1.html#osha_pel1 (Accessed August 8, 2018).
[22] U.S. Department of Labor: Occupational safety and Health administration. Annotated OSHA Z-2 Table n.d. https://www.osha.gov/dsg/annotated-pels/tablez-2.html (Accessed August 8, 2018).
[23] Chen H, Cong TN, Yang W, Tan C, Li Y, Ding Y. Progress in electrical energy storage system: a critical review. Prog Nat Sci 2009;19:291–312. https://doi.org/10.1016/j.pnsc.2008.07.014.
[24] Pellow MA, Emmott CJM, Barnhart CJ, Benson SM. Hydrogen or batteries for grid storage? A net energy analysis. Energy Environ Sci 2015;8:1938–52. https://doi.org/10.1039/c4ee04041d.
[25] U.K. Government. Department of business energy and industrial strategy. Energy Trends and Prices statistical release: 26 July 2018; 2018.
[26] Amos WA. Costs of storing and transporting hydrogen. 1998.
[27] Gahleitner G. Hydrogen from renewable electricity: an international review of power-to-gas pilot plants for stationary applications. Int J Hydrogen Energy 2013;38:2039–61. https://doi.org/10.1016/j.ijhydene.2012.12.010.
[28] Grube T, Doré L, Hoffrichter A, Hombach LE, Raths S, Robinius M, et al. An option for stranded renewables: electrolytic-hydrogen in future energy systems. Sustain Energy Fuels 2018;2:1500–15. https://doi.org/10.1039/C8SE00008E.
[29] Bañares-Alcántara R, Dericks III G, Fiaschetti M, Grunewald P, Masa Lopez J, Tsang E, et al. Analysis of islanded ammonia-based energy storage systems. 2015.
[30] International Energy Agency. Key world energy statistics. 2017.
[31] Isenstadt A, Lutsey N. Developing hydrogen fueling infrastructure for fuel cell vehicles : a status update. 2017.
[32] McKinsey & Company. A portfolio of power-trains for Europe: a fact-based analysis. 2011.
[33] Ministerial council on renewable energy hydrogen and related issues. Basic hydrogen strategy. 2017.
[34] Miyaoka H, Ichikawa T, Hino S, Kojima Y. Compressed hydrogen production via reaction between liquid ammonia and alkali metal hydride. Int J Hydrogen Energy 2011;36:8217–20. https://doi.org/10.1016/j.ijhydene.2011.04.170.
[35] Müller K, Brooks KP, Autrey T. Releasing hydrogen at high pressures from liquid carriers: aspects for the H_2 delivery to fueling stations. Energy Fuels 2018. https://doi.org/10.1021/acs.energyfuels.8b01724.
[36] Eppinger J, Huang K-W. Formic acid as a hydrogen energy carrier. ACS Energy Lett 2017;2:188–95. https://doi.org/10.1021/acsenergylett.6b00574.
[37] Parks G, Boyd R, Cornish J, Remick R. Hydrogen station compression, storage, and dispensing technical Status and costs: systems integration. Int J Hydrogen Energy 2014. https://doi.org/10.2172/1130621.
[38] Lototskyy MV, Yartys VA, Pollet BG, Bowman RC. Metal hydride hydrogen compressors: a review. Int J Hydrogen

Energy 2014;39:5818–51. https://doi.org/10.1016/j.ijhydene.2014.01.158.
[39] Sordakis K, Tang C, Vogt LK, Junge H, Dyson PJ, Beller M, et al. Homogeneous catalysis for sustainable hydrogen storage in formic acid and alcohols. Chem Rev 2018;118:372–433. https://doi.org/10.1021/acs.chemrev.7b00182.
[40] Wang X, Meng Q, Gao L, Jin Z, Ge J, Liu C, et al. Recent progress in hydrogen production from formic acid decomposition. Int J Hydrogen Energy 2018;43:7055–71. https://doi.org/10.1016/j.ijhydene.2018.02.146.
[41] Zhu QL, Xu Q. Liquid organic and inorganic chemical hydrides for high-capacity hydrogen storage. Energy Environ Sci 2015;8:478–512. https://doi.org/10.1039/c4ee03690e.
[42] Demirci UB. Ammonia borane, a material with exceptional properties for chemical hydrogen storage. Int J Hydrogen Energy 2017;42:9978–10013. https://doi.org/10.1016/j.ijhydene.2017.01.154.
[43] Li H, Yang Q, Chen X, Shore SG. Ammonia borane, past as prolog. J Organomet Chem 2014;751:60–6. https://doi.org/10.1016/j.jorganchem.2013.08.044.
[44] Moussa G, Moury R, Demirci UB, Miele P. Borates in hydrolysis of ammonia borane. Int J Hydrogen Energy 2013;38:7888–95. https://doi.org/10.1016/j.ijhydene.2013.04.121.
[45] Demirci UB. The hydrogen cycle with the hydrolysis of sodium borohydride: a statistical approach for highlighting the scientific/technical issues to prioritize in the field. Int J Hydrogen Energy 2015;40:2673–91. https://doi.org/10.1016/j.ijhydene.2014.12.067.
[46] Brack P, Dann SE, Upul Wijayantha KG. Heterogeneous and homogenous catalysts for hydrogen generation by hydrolysis of aqueous sodium borohydride ($NaBH_4$) solutions. Energy Sci Eng 2015;3:174–88. https://doi.org/10.1002/ese3.67.
[47] Erisman JW, Sutton MA, Galloway J, Klimont Z, Winiwarter W. How a century of ammonia synthesis changed the world. Nat Geosci 2008;1:636–9.
[48] Thomas G, Parks G. Potential roles of ammonia in a hydrogen economy. 2006.
[49] Lan R, Irvine JTS, Tao S. Ammonia and related chemicals as potential indirect hydrogen storage materials. Int J Hydrogen Energy 2012;37:1482–94. https://doi.org/10.1016/j.ijhydene.2011.10.004.
[50] Klerke A, Christensen CH, Nørskov JK, Vegge T. Ammonia for hydrogen storage: challenges and opportunities. J Mater Chem 2008;18:2304. https://doi.org/10.1039/b720020j.
[51] Zamfirescu C, Dincer I. Ammonia as a green fuel and hydrogen source for vehicular applications. Fuel Process Technol 2009;90:729–37. https://doi.org/10.1016/j.fuproc.2009.02.004.
[52] Christensen CH, Johannessen T, Sørensen RZ, Nørskov JK. Towards an ammonia-mediated hydrogen economy? Catal Today 2006;111:140–4. https://doi.org/10.1016/j.cattod.2005.10.011.
[53] Zamfirescu C, Dincer I. Using ammonia as a sustainable fuel. J Power Sources 2008;185:459–65. https://doi.org/10.1016/j.jpowsour.2008.02.097.
[54] Brown T. Yara: solar ammonia pilot plant, for start-up in 2019. Ammon Ind n.d. https://ammoniaindustry.com/yara-solar-ammonia-pilot-plant-for-start-up-in-2019/ (Accessed August 9, 2018).
[55] Thyssenkrupp. thyssenkrupp supports Australian Company H2U in green hydrogen and renewable ammonia value chain development n.d. https://www.thyssenkrupp-industrial-solutions.com/en/press_detail_48384.html (Accessed August 9, 2018).
[56] Valera-Medina A, Morris S, Runyon J, Pugh D, Marsh R, Beasley P, et al. Ammonia, methane and hydrogen for gas turbines. Energy Procedia 2015;75:118–23. https://doi.org/10.1016/j.egypro.2015.07.205.
[57] Xiao H, Valera-Medina A, Bowen PJ. Modeling combustion of ammonia/ hydrogen fuel blends under gas turbine conditions. Energy Fuels 2017;31:8631–42. https://doi.org/10.1021/acs.energyfuels.7b00709.
[58] Comotti M, Frigo S. Hydrogen generation system for ammonia-hydrogen fuelled internal combustion engines. Int J Hydrogen Energy 2015;40:10673–86. https://doi.org/10.1016/j.ijhydene.2015.06.080.
[59] Philibert C. Renewable energy for industry: offshore wind in Northern Europe. 2018.
[60] Brown T. Ammonia production causes 1% of total global GHG emissions. Ammon Ind 2016. https://ammoniaindustry.com/ammonia-production-causes-1-percent-of-total-global-ghg-emissions/ (Accessed 13 August 2018).
[61] Institute for Industrial Productivity. Ammonia. Industry Efficiency Technological Database n.d. http://ietd.iipnetwork.org/content/ammonia#benchmarks (Accessed 10 August 2018)
[62] Guo J, Chen P. Catalyst: NH_3 as an energy carrier. Chem 2017;3:709–12. https://doi.org/10.1016/j.chempr.2017.10.004.
[63] Chen JG, Crooks RM, Seefeldt LC, Bren KL, Morris Bullock R, Darensbourg MY, et al. Beyond fossil fuel–driven nitrogen transformations. Science 2018;360. https://doi.org/10.1126/science.aar6611.
[64] Dybkjaer I. Ammonia production processes. In: Nielsen A, editor. Ammonia catalysis and manufacture. Springer; 1995.
[65] Medford AJ, Vojvodic A, Hummelshøj JS, Voss J, Abild-Pedersen F, Studt F, et al. From the Sabatier principle to a predictive theory of transition-metal heterogeneous catalysis. J Catal 2015;328:36–42. https://doi.org/10.1016/j.jcat.2014.12.033.
[66] Munter TR, Bligaard T, Christensen CH, Nørskov JK. BEP relations for N_2 dissociation over stepped transition metal and alloy surfaces. Phys Chem Chem Phys 2008;10:5202–6. https://doi.org/10.1039/b720021h.
[67] Wang P, Chang F, Gao W, Guo J, Wu G, He T, et al. Breaking scaling relations to achieve low-temperature ammonia synthesis through LiH-mediated nitrogen transfer and hydrogenation. Nat Chem 2016:64–70. https://doi.org/10.1038/nchem.2595.
[68] Jacobsen CJH. Novel class of ammonia synthesis catalysts. Chem Commun 2000:1057–8. https://doi.org/10.1039/b002930k.
[69] Zeinalipour-Yazdi CD, Hargreaves JSJ, Catlow CRA. Nitrogen activation in a Mars-van Krevelen mechanism for ammonia synthesis on Co_3Mo_3N. J Phys Chem C 2015;119:28368–76. https://doi.org/10.1021/acs.jpcc.5b06811.
[70] Hargreaves JSJ, McFarlane A, Catlow CRA, Zeinalipour-Yazdi CD, Flavell W, Leontiadou M, et al. Lattice nitrogen reactivity in Co3Mo3N catalysts: understanding the role of surface structure and composition through application of depth resolved XPS and computational modelling, 251. Abstr Pap Am Chem Soc; 2016.
[71] Hunter SM, Gregory DH, Hargreaves JSJ, Duprez D, Bion N. A study of $^{15}N/^{14}N$ isotopic exchange over cobalt molybdenum nitrides. ACS Catal 2013;3:1719–25. https://doi.org/10.1021/cs400336z.
[72] Laassiri S, Zeinalipour-Yazdi CD, Catlow CRA, Hargreaves JSJ. Nitrogen transfer properties in tantalum nitride based materials. Catal Today 2017;286:147–54. https://doi.org/10.1016/j.cattod.2016.06.035.
[73] Laassiri S, Zeinalipour-Yazdi CD, Catlow CRA, Hargreaves JSJ. The potential of manganese nitride based materials as nitrogen transfer reagents for nitrogen

chemical looping. Appl Catal B Environ 2018;223:60–6. https://doi.org/10.1016/j.apcatb.2017.04.073.
[74] Aika K-I. Role of alkali promoter in ammonia synthesis over ruthenium catalysts—effect on reaction mechanism. Catal Today 2017;286:14–20. https://doi.org/10.1016/j.cattod.2016.08.012.
[75] Kitano M, Inoue Y, Yamazaki Y, Hayashi F, Kanbara S, Matsuishi S, et al. Ammonia synthesis using a stable electride as an electron donor and reversible hydrogen store. Nat Chem 2012;4:934–40. https://doi.org/10.1038/nchem.1476.
[76] Kitano M, Kanbara S, Inoue Y, Kuganathan N, Sushko PV, Yokoyama T, et al. Electride support boosts nitrogen dissociation over ruthenium catalyst and shifts the bottleneck in ammonia synthesis. Nat Commun 2015;6:6731. https://doi.org/10.1038/ncomms7731.
[77] Lu Y, Li J, Tada T, Toda Y, Ueda S, Yokoyama T, et al. Water durable electride Y_5Si_3: electronic structure and catalytic activity for ammonia synthesis. J Am Chem Soc 2016;138:3970–3. https://doi.org/10.1021/jacs.6b00124.
[78] Gao W, Wang P, Guo J, Chang F, He T, Wang Q, et al. Barium hydride-mediated nitrogen transfer and hydrogenation for ammonia synthesis: a case study of cobalt. ACS Catal 2017;7:3654–61. https://doi.org/10.1021/acscatal.7b00284.
[79] Abe H, Niwa Y, Kitano M, Inoue Y, Sasase M, Nakao T, et al. Anchoring bond between Ru and N atoms of Ru/Ca_2NH catalyst: crucial for the high ammonia synthesis activity. J Phys Chem C 2017;121:20900–4. https://doi.org/10.1021/acs.jpcc.7b07268.
[80] Kitano M, Inoue Y, Sasase M, Kishida K, Kobayashi Y, Nishiyama K, et al. Self-organized ruthenium–barium core–shell nanoparticles on a mesoporous calcium amide matrix for efficient low-temperature ammonia synthesis. Angew Chem Int Ed 2018;57:2648–52. https://doi.org/10.1002/anie.201712398.
[81] Chang F, Guan Y, Chang X, Guo J, Wang P, Gao W, et al. Alkali and alkaline earth hydrides-driven N_2 activation and transformation over Mn nitride catalyst. J Am Chem Soc 2018;140:14799–806. https://doi.org/10.1021/jacs.8b08334.
[82] Gao W, Guo J, Wang P, Wang Q, Chang F, Pei Q, et al. Production of ammonia via a chemical looping process based on metal imides as nitrogen carriers. Nat Energy 2018;3. https://doi.org/10.1038/s41560-018-0268-z.
[83] Sørensen RZ, Hummelshøj JS, Klerke A, Reves JB, Vegge T, Nørskov JK, et al. Indirect, reversible high-density hydrogen storage in compact metal ammine salts. J Am Chem Soc 2008;130. https://doi.org/10.1021/ja076762c.
[84] Jensen PB, Bialy A, Blanchard D, Lysgaard S, Reumert AK, Quaade UJ, et al. Accelerated DFT-based design of materials for ammonia storage. Chem Mater 2015;27. https://doi.org/10.1021/acs.chemmater.5b00446.
[85] Skúlason E, Bligaard T, Gudmundsdóttir S, Studt F, Rossmeisl J, Abild-Pedersen F, et al. A theoretical evaluation of possible transition metal electro-catalysts for N_2reduction. Phys Chem Chem Phys 2012;14. https://doi.org/10.1039/c1cp22271f.
[86] Abghoui Y, Garden AL, Howalt JG, Vegge T, Skúlason E. Electroreduction of N_2 to ammonia at ambient conditions on mononitrides of Zr, Nb, Cr, and V: a DFT guide for experiments. ACS Catal 2016;6. https://doi.org/10.1021/acscatal.5b01918.
[87] Singh AR, Rohr BA, Schwalbe JA, Cargnello M, Chan K, Jaramillo TF, et al. Electrochemical ammonia synthesis - the selectivity challenge. ACS Catal 2017;7:706–9. https://doi.org/10.1021/acscatal.6b03035.
[88] Howalt JG, Bligaard T, Rossmeisl J, Vegge T. DFT based study of transition metal nano-clusters for electrochemical NH_3 production. Phys Chem Chem Phys 2013;15. https://doi.org/10.1039/c3cp44641g.
[89] Howalt JG, Vegge T. Electrochemical ammonia production on molybdenum nitride nanoclusters. Phys Chem Chem Phys 2013;15. https://doi.org/10.1039/c3cp53160k.
[90] Howalt JG, Vegge T. The role of oxygen and water on molybdenum nanoclusters for electro catalytic ammonia production. Beilstein J Nanotechnol 2014;5. https://doi.org/10.3762/bjnano.5.11.
[91] Zhang X, Kong R-M, Du H, Xia L, Qu F. Highly efficient electrochemical ammonia synthesis *via* nitrogen reduction reactions on a VN nanowire array under ambient conditions. Chem Commun 2018;54:5323–5. https://doi.org/10.1039/C8CC00459E.
[92] Ren X, Cui G, Chen L, Xie F, Wei Q, Tian Z, et al. Electrochemical N_2 fixation to NH_3 under ambient conditions: Mo_2N nanorod as a highly efficient and selective catalyst. Chem Commun 2018;2:8474–7. https://doi.org/10.1039/C8CC03627F.
[93] Cui X, Tang C, Zhang Q. A review of electrocatalytic reduction of dinitrogen to ammonia under ambient conditions. Adv Energy Mater 2018;1800369:1–25. https://doi.org/10.1002/aenm.201800369.
[94] Kim K, Lee SJ, Kim DY, Yoo CY, Choi JW, Kim JN, et al. Electrochemical synthesis of ammonia from water and nitrogen: a lithium-mediated approach using lithium-ion conducting glass ceramics. ChemSusChem 2018;11:120–4. https://doi.org/10.1002/cssc.201701975.
[95] McEnaney JM, Singh AR, Schwalbe JA, Kibsgaard J, Lin JC, Cargnello M, et al. Ammonia synthesis from N_2 and H_2O using a lithium cycling electrification strategy at atmospheric pressure. Energy Environ Sci 2017;10:1621–30. https://doi.org/10.1039/C7EE01126A.
[96] Zhou F, Azofra LM, Al-Agele M, Kar M, Simonov AN, McDonnell-Worth CJ, et al. Electro-synthesis of ammonia from nitrogen at ambient temperature and pressure in ionic liquids. Energy Environ Sci 2017:2516–20. https://doi.org/10.1039/C7EE02716H.
[97] Suryanto BHR, Kang CSM, Wang D, Xiao C, Zhou F, Azofra LM, et al. Rational electrode-electrolyte design for efficient ammonia electrosynthesis under ambient conditions. ACS Energy Lett 2018;3:1219–24. https://doi.org/10.1021/acsenergylett.8b00487.
[98] Lysgaard S, Christensen MK, Hansen HA, García Lastra JM, Norby P, Vegge T. Combined DFT and differential electrochemical mass Spectrometry investigation of the effect of dopants in secondary zinc–air batteries. ChemSusChem 2018;11:1933–41. https://doi.org/10.1002/cssc.201800225.
[99] Hacker V, Kordesch K. Ammonia crackers. In: Vielstich W, Lamm A, Gasteiger HA, editors. Handb. Fuel cells - Fundam. Technol. Appl., vol. 3. Chichester: John Wiley & Sons, Ltd; 2003. p. 121–7.
[100] Schüth F, Palkovits R, Schlögl R, Su DS. Ammonia as a possible element in an energy infrastructure: catalysts for ammonia decomposition. Energy Environ Sci 2012;5:6278. https://doi.org/10.1039/c2ee02865d.
[101] Yin SF, Xu BQ, Zhou XP, Au CT. A mini-review on ammonia decomposition catalysts for on-site generation of hydrogen for fuel cell applications. Appl Catal A Gen 2004;277:1–9. https://doi.org/10.1016/j.apcata.2004.09.020.
[102] Bell TE, Torrente-Murciano L. H_2 production via ammonia decomposition using non-noble metal catalysts: a review. Top Catal 2016:1–20. https://doi.org/10.1007/s11244-016-0653-4.
[103] Mukherjee S, Devaguptapu SV, Sviripa A, Lund CRF, Wu G. Low-temperature ammonia decomposition catalysts for

hydrogen generation. Appl Catal B 2018;226:162–81. https://doi.org/10.1016/j.apcatb.2017.12.039.
[104] Anilin Badische, Soda Fabrik. Varfahren zur synthetischen Darstellung von Ammoniak aus den Elementen. 1908. 235421.
[105] Kunsman CH. The decomposition of ammonia on iron catalysts. Science 1927;65:527–8. https://doi.org/10.1126/science.77.1989.173-a.
[106] Kunsman CH. The thermal decomposition of ammonia on iron catalysts. II. J Am Chem Soc 1929;51:688–95. https://doi.org/10.1021/ja01378a005.
[107] Love KS, Emmett PH. The catalytic decomposition of ammonia over iron synthetic ammonia catalysts. J Am Chem Soc 1941;63:3297–308. https://doi.org/10.1021/ja01857a019.
[108] Brunauer S, Love KS, Keenan RG. Adsorption of nitrogen and the mechanism of ammonia decomposition over iron catalysts*. J Am Chem Soc 1942;64:751–8. https://doi.org/10.1021/ja01256a005.
[109] Schwab GM, Krabetz R. Kinetik der ammoniakzersetzung an eisen. Zeitschrift Fur Elektrochemie 1956;60:855–9.
[110] Takezawa N, Toyoshima I. The change of the rate-determining step of the ammonia decomposition over an ammonia synthetic iron catalyst. J Phys Chem 1966;70:594–5. https://doi.org/10.1021/j100874a509.
[111] Löffler DG, Schmidt LD. Kinetics of NH_3 decomposition on iron at high temperatures. J Catal 1976;44:244–58. https://doi.org/10.1016/0021-9517(76)90395-X.
[112] Ertl G, Huber M. Mechanism and kinetics of ammonia decomposition on iron. J Catal 1980;61:537–9. https://doi.org/10.1016/0021-9517(80)90403-0.
[113] Bradford MCJ, Fanning PE, Vannice MA. Kinetics of NH_3 decomposition over well dispersed Ru. J Catal 1997;172:479–84.
[114] Arabczyk W, Zamłynny J. Study of the ammonia decomposition over iron catalysts. Catal Letters 1999;60:167–71. https://doi.org/10.1023/A:1019007024041.
[115] Tamaru K. Adsorption measurements during the decomposition of ammonia on a tungsten catalyst. Trans Faraday Soc 1961;57:1410–5. https://doi.org/10.1039/TF9615701410.
[116] Tamaru K, Tanaka K-I, Fukasaku S, Ishida S. Decomposition of ammonia on a nickel catalyst. Trans Faraday Soc 1965;61:765–72. https://doi.org/10.1039/tf9656100765.
[117] Choudhary TV, Sivadinarayana C, Goodman DW. Production of CO_x -free hydrogen for fuel cells via step-wise hydrocarbon reforming and catalytic dehydrogenation of ammonia. Chem Eng J 2003;93:69–80. https://doi.org/10.1016/S1385-8947(02)00110-9.
[118] Yin S-F, Zhang Q-H, Xu B, Zhu W-X, Ng C-F, Au C-T. Investigation on the catalysis of CO_x -free hydrogen generation from ammonia. J Catal 2004;224:384–96. https://doi.org/10.1016/j.jcat.2004.03.008.
[119] Yin S, Xu B, Ng C, Au C. Nano Ru/ CNTs : a highly active and stable catalyst for the generation of CO $_x$ -free hydrogen in ammonia decomposition. Appl Catal B Environ 2004;48:237–41. https://doi.org/10.1016/j.apcatb.2003.10.013.
[120] Raróg-Pilecka W, Szmigiel D, Komornicki A, Zieliński J, Kowalczyk Z. Catalytic properties of small ruthenium particles deposited on carbon: ammonia decomposition studies. Carbon 2003;41:589–91. https://doi.org/10.1016/S0008-6223(02)00393-7.
[121] Raróg-Pilecka W, Miśkiewicz E, Szmigiel D, Kowalczyk Z. Structure sensitivity of ammonia synthesis over promoted ruthenium catalysts supported on graphitised carbon. J Catal 2005;231:11–9. https://doi.org/10.1016/j.jcat.2004.12.005.
[122] Li L, Zhu ZH, Yan ZF, Lu GQ, Rintoul L. Catalytic ammonia decomposition over Ru/carbon catalysts: the importance of the structure of carbon support. Appl Catal A Gen 2007;320:166–72. https://doi.org/10.1016/j.apcata.2007.01.029.
[123] Jedynak A, Kowalczyk Z, Szmigiel D, Raróg W, Zielinski J. Ammonia decomposition over the carbon-based iron catalyst promoted with potassium. Appl Catal A Gen 2002;237:223–6.
[124] Kowalczyk Z, Sentek J, Jodzis S, Muhler M, Hinrichsen O. Effect of potassium on the kinetics of ammonia synthesis and decomposition over fused iron catalyst at atmospheric pressure. J Catal 1997;414:407–14. https://doi.org/10.1006/jcat.1997.1664.
[125] Raróg-Pilecka W, Szmigiel D, Kowalczyk Z, Jodzis S, Zielinski J. Ammonia decomposition over the carbon-based ruthenium catalyst promoted with barium or cesium. J Catal 2003;218:465–9. https://doi.org/10.1016/S0021-9517(03)00058-7.
[126] Saadatjou N, Jafari A, Sahebdelfar S. Ruthenium nanocatalysts for ammonia synthesis: a review. Chem Eng Commun 2015;202:420–48. https://doi.org/10.1080/00986445.2014.923995.
[127] García-García FR, Guerrero-Ruiz A, Rodríguez-Ramos I. Role of B5-type Sites in Ru catalysts used for the NH_3 decomposition reaction. Top Catal 2009;52:758–64. https://doi.org/10.1007/s11244-009-9203-7.
[128] Okura K, Okanishi T, Muroyama H, Matsui T, Eguchi K. Promotion effect of rare-earth elements on the catalytic decomposition of ammonia over Ni/Al_2O_3 catalyst. Appl Catal A Gen 2015;505:77–85. https://doi.org/10.1016/j.apcata.2015.07.020.
[129] Zhang J, Muller J, Zheng W, Wang D, Su D, Schlögl R. Individual Fe - Co alloy nanoparticles on carbon Nanotubes : structural and catalytic properties. Nano Lett 2008;8:2738–43. https://doi.org/10.1021/nl8011984.
[130] Wood TJ, Makepeace JW, David WIF. Neutron diffraction and gravimetric study of the iron nitriding reaction under ammonia decomposition conditions. Phys Chem Chem Phys 2017;19:27859–65. https://doi.org/10.1039/C7CP07613D.
[131] Tseng J-C, Gu D, Pistidda C, Horstmann C, Dornheim M, Ternieden J, et al. tracking the active catalyst for iron-based ammonia decomposition by in situ Synchrotron diffraction studies. ChemCatChem 2018. https://doi.org/10.1002/cctc.201800398.
[132] Tagliazucca V, Schlichte K, Schüth F, Weidenthaler C. Molybdenum-based catalysts for the decomposition of ammonia: in situ X-ray diffraction studies, microstructure, and catalytic properties. J Catal 2013;305:277–89. https://doi.org/10.1016/j.jcat.2013.05.011.
[133] Gu Y-Q, Fu X-P, Du P, Gu D, Jin Z, Huang Y-Y, et al. In situ X-ray diffraction study of Co-Al nanocomposites as catalysts for ammonia decomposition. J Phys Chem C 2015;119:17102–10. https://doi.org/10.1021/acs.jpcc.5b02932.
[134] Wood TJ, Makepeace JW, David WIF. Neutron diffraction and gravimetric study of the manganese nitriding reaction under ammonia decomposition conditions. Phys Chem Chem Phys 2018;20:8547–53. https://doi.org/10.1039/C7CP07613D.
[135] Li Y, Liu S, Yao L, Ji W, Au CT. Core-shell structured iron nanoparticles for the generation of CO_x-free hydrogen via ammonia decomposition. Catal Commun 2010;11:368–72. https://doi.org/10.1016/j.catcom.2009.11.003.
[136] Feyen M, Weidenthaler C, Güttel R, Schlichte K, Holle U, Lu A-H, et al. High-temperature stable, iron-based core-shell catalysts for ammonia decomposition. Chem Eur J 2011;17:598–605. https://doi.org/10.1002/chem.201001827.
[137] Pansare SS, Torres W, Goodwin Jr JG. Ammonia decomposition on tungsten carbide. Catal Commun 2007;8:649–54. https://doi.org/10.1016/j.catcom.2006.08.016.

[138] Cui X, Li H, Guo L, He D, Chen H, Shi J. Synthesis of mesoporous tungsten carbide by an impregnation-compaction route, and its NH_3 decomposition catalytic activity. Dalt Trans 2008:6435–40. https://doi.org/10.1039/b809923e.
[139] Choi J-G. Ammonia decomposition over vanadium carbide catalysts. J Catal 1999;182:104–16. https://doi.org/10.1006/jcat.1998.2346.
[140] Titherley AW. Sodium, potassium, and lithium amides. J Chem Soc 1894;65:504–22. https://doi.org/10.1039/CT8946500504.
[141] Chen P, Xiong Z, Luo J, Lin J, Tan KL. Interaction of hydrogen with metal nitrides and imides. Nature 2002;420:302–4. https://doi.org/10.1038/nature01210.
[142] Chen P, Xiong Z, Wu G, Liu Y, Hu J, Luo W. Metal–N–H systems for the hydrogen storage. Scr Mater 2007;56:817–22. https://doi.org/10.1016/j.scriptamat.2007.01.001.
[143] Xiong Z, Wu G, Hu J, Chen P. Ternary imides for hydrogen storage. Adv Mater 2004;16:1522–5. https://doi.org/10.1002/adma.200400571.
[144] David WIF, Makepeace JW, Callear SK, Hunter HMA, Taylor JD, Wood TJ, et al. Hydrogen production from ammonia using sodium amide. J Am Chem Soc 2014;136:13082–5. https://doi.org/10.1021/ja5042836.
[145] Guo J, Wang P, Wu G, Wu A, Hu D, Xiong Z, et al. Lithium imide synergy with 3d transition-metal nitrides leading to unprecedented catalytic activities for ammonia decomposition. Angew Chemie Int Ed 2015;127:2993–7. https://doi.org/10.1002/ange.201410773.
[146] Makepeace JW, Wood TJ, Hunter HMA, Jones MO, David WIF. Ammonia decomposition catalysis using non-stoichiometric lithium imide. Chem Sci 2015;6:3805–15. https://doi.org/10.1039/C5SC00205B.
[147] Guo J, Chang F, Wang P, Hu D, Yu P, Wu G, et al. Highly active MnN–Li_2NH composite catalyst for producing CO_x -free hydrogen. ACS Catal 2015;5:2708–13. https://doi.org/10.1021/acscatal.5b00278.
[148] Chang F, Guo J, Wu G, Wang P, Yu P, Chen P. Influence of alkali metal amides on the catalytic activity of manganese nitride for ammonia decomposition. Catal Today 2017;286:141–6. https://doi.org/10.1016/j.cattod.2016.09.010.
[149] Makepeace JW, Hunter HMA, Wood TJ, Smith RI, Murray CA, David WIF. Ammonia decomposition catalysis using lithium-calcium imide. Faraday Discuss 2016;188:525–44. https://doi.org/10.1039/C5FD00179J.
[150] Yu P, Guo J, Liu L, Wang P, Chang F, Wang H, et al. Effects of alkaline earth metal amides on Ru in catalytic ammonia decomposition. J Phys Chem C 2016;120:2822–8. https://doi.org/10.1021/acs.jpcc.5b11768.
[151] Cao H, Guo J, Chang F, Pistidda C, Zhou W, Zhang X, et al. Transition and alkali metal complex ternary amides for ammonia synthesis and decomposition. Chem Eur J 2017;23:9766–71. https://doi.org/10.1002/chem.201702728.
[152] Aika KA, Kawahara TSM, Onishi T. Promoter effect of alkali metal oxides and alkali earth metal oxides on active carbon-supported ruthenium catalyst for ammonia synthesis. Bull Chem Soc Jpn 1990;63:1221–5.
[153] Guo J, Chen Z, Wu A, Chang F, Wang P, Hu D, et al. Electronic promoter or reacting species? The role of $LiNH_2$ on Ru in catalyzing NH_3 decomposition. Chem Commun 2015;51:15161–4. https://doi.org/10.1039/C5CC04645A.
[154] Bellosta von Colbe JM, Metz O, Lozano G a, Pranzas PK, Schmitz HW, Beckmann F, et al. Behavior of scaled-up sodium alanate hydrogen storage tanks during sorption. Int J Hydrogen Energy 2012;37:2807–11. https://doi.org/10.1016/j.ijhydene.2011.03.153.
[155] Yu P, Guo J, Liu L, Wang P, Wu G, Chang F, et al. Ammonia decomposition with manganese nitride – calcium imide composites as efficient catalysts. ChemSusChem 2016;9:364–9. https://doi.org/10.1002/cssc.201501498.
[156] Marx R. Preparation and crystal structure of lithium nitride hydride, Li_4NH, Li_4ND. Z Anorg Allg Chem 1997;623:1912–6. https://doi.org/10.1002/chin.199813003.
[157] Peikun W, Guo J, Chen P. The interactions of Li_3FeN_2 with H_2 and NH_3 ScienceDirect. Int J Hydrogen Energy 2016:1–7. https://doi.org/10.1016/j.ijhydene.2016.05.108.
[158] Makepeace JW, Wood TJ, Marks PL, Smith RI, Murray CA, David WIF. Bulk phase behavior of lithium imide–metal nitride ammonia decomposition catalysts. Phys Chem Chem Phys 2018. https://doi.org/10.1039/C8CP02824A.
[159] Wood TJ, Makepeace JW. Assessing potential supports for lithium amide-imide ammonia decomposition catalysts. ACS Appl Energy Mater 2018;1:2657–63. https://doi.org/10.1021/acsaem.8b00351.
[160] Consultants Quest. Comparative quantitative risk analysis of motor gasoline, LPG, and anhydrous ammonia as an automotive fuel. 2009.
[161] Duijm NJ, Markert F, Paulsen JL. Safety assessment of ammonia as a transport fuel. 2005.
[162] Christensen CH, Sørensen RZ, Johannessen T, Quaade UJ, Honkala K, Elmøe TD, et al. Metal ammine complexes for hydrogen storage. J Mater Chem 2005;15:4106. https://doi.org/10.1039/b511589b.
[163] Vegge T, Sørensen RZ, Klerke A, Hummelshøj JS, Johannessen T, Nørskov JK. Indirect hydrogen storage in metal ammines. In: Walker G, editor. Solid-State hydrogen storage. Woodhead Publishing; 2008. https://doi.org/10.1533/9781845694944.4.533.
[164] Jensen PB, Lysgaard S, Quaade UJ, Vegge T. Designing mixed metal halide ammines for ammonia storage using density functional theory and genetic algorithms. Phys Chem Chem Phys 2014;16. https://doi.org/10.1039/c4cp03133d.
[165] Hjorth Larsen A, JØrgen Mortensen J, Blomqvist J, Castelli IE, Christensen R, Dułak M, et al. The atomic simulation environment - a Python library for working with atoms. J Phys Condens Matter 2017;29. https://doi.org/10.1088/1361-648X/aa680e.
[166] Bialy A, Jensen PB, Blanchard D, Vegge T, Quaade UJ. Solid solution barium-strontium chlorides with tunable ammonia desorption properties and superior storage capacity. J Solid State Chem 2015;221. https://doi.org/10.1016/j.jssc.2014.09.014.
[167] Ammitzboll AL, Lysgaard S, Klukowska A, Vegge T, Quaade UJ. Surface adsorption in strontium chloride ammines. J Chem Phys 2013;138. https://doi.org/10.1063/1.4800754.
[168] Tekin A, Hummelshøj JS, Jacobsen HS, Sveinbjörnsson D, Blanchard D, Nørskov JK, et al. Ammonia dynamics in magnesium ammine from DFT and neutron scattering. Energy Environ Sci 2010;3. https://doi.org/10.1039/b921442a.
[169] Lysgaard S, Ammitzbøll AL, Johnsen RE, Norby P, Quaade UJ, Vegge T. Resolving the stability and structure of strontium chloride amines from equilibrium pressures, XRD and DFT. Int J Hydrogen Energy 2012;37:18927–36.
[170] Johnsen RE, Jensen PB, Norby P, Vegge T. Temperature- and pressure-induced changes in the crystal structure of $Sr(NH_3)_8Cl_2$. J Phys Chem C 2014;118. https://doi.org/10.1021/jp508076c.
[171] Paskevicius M, Jepsen LH, Schouwink P, Černý R, Ravnsbæk DB, Filinchuk Y, et al. Metal borohydrides and derivatives-synthesis, structure and properties. Chem Soc Rev 2017;46:1565–634. https://doi.org/10.1039/c6cs00705h.
[172] Jepsen LH, Ley MB, Lee Y-S, Cho YW, Dornheim M, Jensen JO, et al. Boron-nitrogen based hydrides and reactive composites for hydrogen storage. Mater Today

2014;17:129–35. https://doi.org/10.1016/j.mattod.2014.02.015.
[173] Černý R, Schouwink P. The crystal chemistry of inorganic metal boro-hydrides and their relation to metal oxides. Acta Crystallogr Sect B Struct Sci Cryst Eng Mater 2015;71:619–40. https://doi.org/10.1107/S2052520615018508.
[174] Jepsen LH, Ley MB, Černý R, Lee Y-S, Cho YW, Ravnsbæk D, et al. Trends in syntheses, structures, and properties for three series of ammine rare-earth metal borohydrides, $M(BH_4)_3 \cdot nNH_3$ (M = Y, Gd, and Dy). Inorg Chem 2015;54:7402–14. https://doi.org/10.1021/acs.inorgchem.5b00951.
[175] Soloveichik G, Her JH, Stephens PW, Gao Y, Rijssenbeek J, Andrus M, et al. Ammine magnesium borohydride complex as a new material for hydrogen storage: structure and properties of $Mg(BH_4)_2$. $2NH_3$. Inorg Chem 2008;47:4290–8. https://doi.org/10.1021/ic7023633.
[176] Jepsen LH, Ley MB, Filinchuk Y, Besenbacher F, Jensen TR. Tailoring the properties of ammine metal borohydrides for solid-state hydrogen storage. ChemSusChem 2015;8:1452–63. https://doi.org/10.1002/cssc.201500029.
[177] Jepsen LH, Lee Y-S, Černý R, Sarusie RS, Cho YW, Besenbacher F, et al. Ammine calcium and strontium borohydrides: syntheses, structures, and properties. ChemSusChem 2015;8:3472–82. https://doi.org/10.1002/cssc.201500713.
[178] Filinchuk Y, Hagemann H. Structure and properties of $NaBH_4 \cdot 2H_2O$ and $NaBH_4$. Eur J Inorg Chem 2008:3127–33. https://doi.org/10.1002/ejic.200800053.
[179] Gu Q, Gao L, Guo Y, Tan Y, Tang Z, Wallwork KS, et al. Structure and decomposition of zinc borohydride ammonia adduct: towards a pure hydrogen release. Energy Environ Sci 2012;5:7590–600. https://doi.org/10.1039/c2ee02485c.
[180] Ravnsbæk D, Filinchuk Y, Cerenius Y, Jakobsen HJ, Besenbacher F, Skibsted J, et al. A series of mixed-metal borohydrides. Angew Chem Ed 2009;48:6659–63. https://doi.org/10.1002/anie.200903030.
[181] Uribe FA, Gottesfeld S, Zawodzinski TA. Effect of ammonia as potential fuel impurity on proton exchange membrane fuel cell performance. J Electrochem Soc 2002;149:A293. https://doi.org/10.1149/1.1447221.
[182] Ohi JM, Vanderborgh N, Gerald Voecks Consultants. Hydrogen fuel quality specifications for polymer electrolyte fuel cells in road vehicles. 2016.
[183] Kordesch K, Cifrain M. A comparison between the alkaline fuel cell (AFC) and the polymer electrolyte membrane (PEM) fuel cell. In: Vielstich W, Lamm A, Gasteiger HA, editors. Handb. Fuel cells – Fundam. Technol. Appl., vol. 4. Chichester: John Wiley & Sons, Ltd; 2003. p. 789–93.
[184] Chase Jr MW. In: NIST-JANAF thermochemical tables. 4th ed. American Institute of Physics; 1998.
[185] Miyaoka H, Miyaoka H, Ichikawa T, Ichikawa T, Kojima Y. Highly purified hydrogen production from ammonia for PEM fuel cell. Int J Hydrogen Energy 2018;43:14486–92. https://doi.org/10.1016/j.ijhydene.2018.06.065.
[186] Van Hassel BA, Karra JR, Santana J, Saita S, Murray A, Goberman D, et al. Ammonia sorbent development for on-board H_2 purification. Sep Purif Technol 2015;142:215–26. https://doi.org/10.1016/j.seppur.2014.12.009.
[187] Dolan MD, Viano DM, Langley MJ, Lamb KE. Tubular vanadium membranes for hydrogen purification. J Memb Sci 2018;549:306–11. https://doi.org/10.1016/j.memsci.2017.12.031.
[188] Lamb KE, Viano DM, Langley MJ, Hla SS, Dolan MD. High-purity H_2 produced from NH_3 via a ruthenium-based decomposition catalyst and vanadium-based membrane. Ind Eng Chem Res 2018:8–13. https://doi.org/10.1021/acs.iecr.8b01476.
[189] Crabtree RH. Hydrogen storage in liquid organic heterocycles. Energy Environ Sci 2008;1:134–8. https://doi.org/10.1039/b805644g.
[190] Pez GP, Scott AR, Cooper AC, Cheng H, Wilhelm FC, Abdourazak AH. Hydrogen storage by reversible hydrogenation of pi-conjugated substrates. 2003. US7351395B1.
[191] Teichmann D, Stark K, Müller K, Zöttl G, Wasserscheid P, Arlt W. Energy storage in residential and commercial buildings via liquid organic hydrogen carriers (LOHC). Energy Environ Sci 2012;5:9044–54. https://doi.org/10.1039/c2ee22070a.
[192] Sakintuna B, Lamari-Darkrim F, Hirscher M. Metal hydride materials for solid hydrogen storage: a review. Int J Hydrogen Energy 2007;32:1121–40. https://doi.org/10.1016/j.ijhydene.2006.11.022.
[193] Clot E, Eisenstein O, Crabtree RH. Computational structure-activity relationships in H_2 storage: how placement of N atoms affects release temperatures in organic liquid storage materials. Chem Commun 2007:2231–3. https://doi.org/10.1039/b705037b.
[194] Pez GP, Scott AR, Cooper AC, Cheng H. Hydrogen storage by reversible hydrogenation of pi-conjugated substrates. 2003. US7101530B2.
[195] Amende M, Schernich S, Sobota M, Nikiforidis I, Hieringer W, Assenbaum D, et al. Dehydrogenation mechanism of liquid organic hydrogen carriers: dodecahydro-N-ethylcarbazole on Pd(111). Chem Eur J 2013;19:10854–65. https://doi.org/10.1002/chem.201301323.
[196] Amende M, Gleichweit C, Werner K, Schernich S, Zhao W, Lorenz MPA, et al. Model catalytic studies of liquid organic hydrogen carriers: dehydrogenation and decomposition mechanisms of dodecahydro-N-ethylcarbazole on Pt(111). ACS Catal 2014;4:657–65. https://doi.org/10.1021/cs400946x.
[197] Gleichweit C, Amende M, Schernich S, Zhao W, Lorenz MPA, Höfert O, et al. Dehydrogenation of dodecahydro-N-ethylcarbazole on Pt(111). ChemSusChem 2013;6:974–7. https://doi.org/10.1002/cssc.201300263.
[198] Cui Y, Kwok S, Bucholtz A, Davis B, Whitney RA, Jessop PG. The effect of substitution on the utility of piperidines and octahydroindoles for reversible hydrogen storage. New J Chem 2008;32:1027–37. https://doi.org/10.1039/b718209k.
[199] Moores A, Poyatos M, Luo Y, Crabtree RH. Catalysed low temperature H_2 release from nitrogen heterocycles. New J Chem 2006;30:1675–8. https://doi.org/10.1039/b608914c.
[200] Fang M, Sánchez-Delgado RA. Ruthenium nanoparticles supported on magnesium oxide: a versatile and recyclable dual-site catalyst for hydrogenation of mono- and polycyclic arenes, N-heteroaromatics, and S-heteroaromatics. J Catal 2014;311:357–68. https://doi.org/10.1016/j.jcat.2013.12.017.
[201] Rahi R, Fang M, Ahmed A, Sánchez-Delgado RA. Hydrogenation of quinolines, alkenes, and biodiesel by palladium nanoparticles supported on magnesium oxide. Dalt Trans 2012;41:14490–7. https://doi.org/10.1039/c2dt31533e.
[202] Sánchez A, Fang M, Ahmed A, Sánchez-Delgado RA. Hydrogenation of arenes, N-heteroaromatic compounds, and alkenes catalyzed by rhodium nanoparticles supported on magnesium oxide. Appl Catal A Gen 2014;477:117–24. https://doi.org/10.1016/j.apcata.2014.03.009.
[203] He T, Liu L, Wu G, Chen P. Covalent triazine framework-supported palladium nanoparticles for catalytic hydrogenation of N-heterocycles. J Mater Chem A 2015;3:16235–41. https://doi.org/10.1039/c5ta03056k.
[204] Deraedt C, Ye R, Ralston WT, Toste FD, Somorjai GA. Dendrimer-stabilized metal nanoparticles as efficient

catalysts for reversible dehydrogenation/hydrogenation of N-heterocycles. J Am Chem Soc 2017;139:18084–92. https://doi.org/10.1021/jacs.7b10768.
[205] Sotoodeh F, Zhao L, Smith KJ. Kinetics of H_2 recovery from dodecahydro-N-ethylcarbazole over a supported Pd catalyst. Appl Catal A Gen 2009;362:155–62. https://doi.org/10.1016/j.apcata.2009.04.039.
[206] Eblagon KM, Tam K, Tsang SCE. Comparison of catalytic performance of supported ruthenium and rhodium for hydrogenation of 9-ethylcarbazole for hydrogen storage applications. Energy Environ Sci 2012;5:8621–30. https://doi.org/10.1039/c2ee22066k.
[207] Sotoodeh F, Huber BJM, Smith KJ. The effect of the N atom on the dehydrogenation of heterocycles used for hydrogen storage. Appl Catal A Gen 2012;419–420:67–72. https://doi.org/10.1016/j.apcata.2012.01.013.
[208] Sotoodeh F, Huber BJM, Smith KJ. Dehydrogenation kinetics and catalysis of organic heteroaromatics for hydrogen storage. Int J Hydrogen Energy 2012;37:2715–22. https://doi.org/10.1016/j.ijhydene.2011.03.055.
[209] Sotoodeh F, Smith KJ. Structure sensitivity of dodecahydro-N-ethylcarbazole dehydrogenation over Pd catalysts. J Catal 2011;279:36–47. https://doi.org/10.1016/j.jcat.2010.12.022.
[210] Yang M, Han C, Ni G, Wu J, Cheng H. Temperature controlled three-stage catalytic dehydrogenation and cycle performance of perhydro-9-ethylcarbazole. Int J Hydrogen Energy 2012;37:12839–45. https://doi.org/10.1016/j.ijhydene.2012.05.092.
[211] Eblagon KM, Tam K, Yu KMK, Tsang SCE. Comparative study of catalytic hydrogenation of 9-ethylcarbazole for hydrogen storage over noble metal surfaces. J Phys Chem C 2012;116:7421–9. https://doi.org/10.1021/jp212249g.
[212] Eblagon KM, Rentsch D, Friedrichs O, Remhof A, Zuettel A, Ramirez-Cuesta AJ, et al. Hydrogenation of 9-ethylcarbazole as a prototype of a liquid hydrogen carrier. Int J Hydrogen Energy 2010;35:11609–21. https://doi.org/10.1016/j.ijhydene.2010.03.068.
[213] Eblagon KM, Tam K, Yu KMK, Zhao S-LL, Gong X-Q, He H, et al. Study of catalytic Sites on ruthenium for hydrogenation of N -ethylcarbazole: implications of hydrogen storage via reversible catalytic hydrogenation. J Phys Chem C 2010;114:9720–30. https://doi.org/10.1021/jp908640k.
[214] Eblagon KM, Tsang SCE. Structure-reactivity relationship in catalytic hydrogenation of heterocyclic compounds over ruthenium black-Part A: effect of substitution of pyrrole ring and side chain in N-heterocycles. Appl Catal B Environ 2014;160–161:22–34. https://doi.org/10.1016/j.apcatb.2014.04.044.
[215] Wang Z, Tonks I, Belli J, Jensen CM. Dehydrogenation of N-ethyl perhydrocarbazole catalyzed by PCP pincer iridium complexes: evaluation of a homogenous hydrogen storage system. J Organomet Chem 2009;694:2854–7. https://doi.org/10.1016/j.jorganchem.2009.03.052.
[216] Wang Z, Belli J, Jensen CM. Homogeneous dehydrogenation of liquid organic hydrogen carriers catalyzed by an iridium PCP complex. Faraday Discuss 2011;151:297. https://doi.org/10.1039/c1fd00002k.
[217] Yamaguchi R, Ikeda C, Takahashi Y, Fujita K-I. Homogeneous catalytic system for reversible dehydrogenation-hydrogenation reactions of nitrogen heterocycles with reversible interconversion of catalytic species. J Am Chem Soc 2009;131:8410–2. https://doi.org/10.1021/ja9022623.
[218] Fujita K, Tanaka Y, Kobayashi M, Yamaguchi R. Homogeneous perdehydrogenation and perhydrogenation of fused bicyclic N-heterocycles catalyzed by iridium complexes bearing a functional bipyridonate ligand. J Am Chem Soc 2014;136:4829–32. https://doi.org/10.1021/ja5001888.
[219] Wu J, Talwar D, Johnston S, Yan M, Xiao J. Acceptorless dehydrogenation of nitrogen heterocycles with a versatile iridium catalyst. Angew Chem Ed 2013;52:6983–7. https://doi.org/10.1002/anie.201300292.
[220] Talwar D, Gonzalez-De-Castro A, Li HY, Xiao J. Regioselective acceptorless dehydrogenative coupling of N-heterocycles toward functionalized quinolines, phenanthrolines, and indoles. Angew Chem Int Ed 2015;54:5223–7. https://doi.org/10.1002/anie.201500346.
[221] Manas MG, Sharninghausen LS, Lin E, Crabtree RH. Iridium catalyzed reversible dehydrogenation - hydrogenation of quinoline derivatives under mild conditions. J Organomet Chem 2015;792:184–9. https://doi.org/10.1016/j.jorganchem.2015.04.015.
[222] Chakraborty S, Brennessel WW, Jones WD. A molecular iron catalyst for the acceptorless dehydrogenation and hydrogenation of N-heterocycles. J Am Chem Soc 2014;136:8564–7. https://doi.org/10.1021/ja504523b.
[223] Bellows SM, Chakraborty S, Gary JB, Jones WD, Cundari TR. An uncanny dehydrogenation mechanism: polar bond control over stepwise or concerted transition states. Inorg Chem 2017;56:5519–24. https://doi.org/10.1021/acs.inorgchem.6b01800.
[224] Xu R, Chakraborty S, Yuan H, Jones WD. Acceptorless, reversible dehydrogenation and hydrogenation of N-heterocycles with a cobalt pincer catalyst. ACS Catal 2015;5:6350–4. https://doi.org/10.1021/acscatal.5b02002.
[225] Luca OR, Huang DL, Takase MK, Crabtree RH. Redox-active cyclopentadienyl Ni complexes with quinoid N-heterocyclic carbene ligands for the electrocatalytic hydrogen release from chemical fuels. New J Chem 2013;37:3402–5. https://doi.org/10.1039/c3nj00276d.
[226] He K-H, Tan F-F, Zhou C-Z, Zhou G-J, Yang X-L, Li Y. Acceptorless dehydrogenation of N-heterocycles by merging visible-light photoredox catalysis and cobalt catalysis. Angew Chem Int Ed 2017;56:3080–4. https://doi.org/10.1002/anie.201612486.